



**University of Vigo and JSPS Core-to
Core Program Joint Seminar**

**“Atomically
Controlled Processing
for Ultralarge Scale
Integration”**

Vigo, September 4th-6th, 2012



Session Index

General Introductions..... 1

General Information on research lines of possible interest at the Laser Group of the University of Vigo.....1

Stefano Chiussi, Pío González, Julia Serra
New Material Group, University of Vigo (Spain)

Laser processing and synthesis of materials at micro- and nanoscale..... 3

Juan Pou, Fernando Lusquiños, Felix Quintero, Mohammed Boutinguiza, Rafael Comesaña, Antonio Riveiro, Jesus del Val
Industrial Applications of Lasers Group, University of Vigo (Spain)

Si and SiGe based materials 7

Atomically Controlled Formation of Strained Si_{1-x}Ge_x/Si Quantum Heterostructure for Room-Temperature Resonant Tunneling Diode.....5

Masao Sakuraba, Junichi Murota
Tohoku University (Japan)

Charge Storage and Optoelectronic Response of Silicide-Nanodots/Si Quantum-Dots Hybrid-Floating-Gate MOS Devices.....7

Seiichi Miyazaki¹, Katsunori Makihara¹, Mitsuhsa Ikeda²
¹Nagoya University, ²Hiroshima University (Japan)

Optical studies of Ge/Si based heterostructures and self-interstitials related defects in Si.....9

Joaquim Leitao
Departamento de Física & I3N, Universidade de Aveiro (Portugal)

Low threading dislocation density Ge growth and heavy phosphorus doping in Ge.....11

Yuji Yamamoto¹, Peter Zaumseil¹, Grzegorz Kozłowski¹, Rainer Kurps¹, Bernd Tillack^{1,2}
¹IHP, Frankfurt an der Oder (Germany), ²Technische Universität Berlin (Germany)

SiGeSn based and other materials..... 13

Epitaxial Growth and Characterizations of GeSn and GeSiSn Thin Layers for Nanoelectronic and Optoelectronic Applications13

Osamu Nakatsuka, Noriyuki Taoka, Mitsuo Sakashita, Wakana Takeuchi, Shigeaki Zaima
Nagoya University (Japan)

Epitaxial Growth of Ge_{1-x}Sn_x with high Sn content by Reduced Pressure CVD15

Stephan Wirths, Dan Buca, Andreas T. Tiedemann, Bernd Holländer, Patric Bernardy, Toma Stoica, Detlev Grützmacher, Sigfried Mantl
Forschungszentrum Jülich (Germany)

FIB preparation and TEM characterization of Ge/Sn based alloys	17
Alessandro Benedetti*, Stefan Stefanov, Julia Serra, Pio González, Stefano Chiussi <i>New Materials Group, *CACTI, University of Vigo (Spain)</i>	
Laser processing of heteroepitaxial GeSn and SiGeSn alloys	18
Stefan Stefanov, Carlos Conde, Carmen Serra*, Alessandro Benedetti*, Stefano Chiussi <i>New Materials Group, *CACTI, University of Vigo (Spain)</i>	
Modelling, applications, and other materials	20
Fabrication of Titanium Oxide Nanotube Micro Gas Sensors by Anodization	20
Yasuo Kimura, Ryota Kojima, Shota Kimura, Michio Niwano <i>Tohoku University (Japan)</i>	
Application of titanium oxide nanotube films to solar cells	21
Michio Niwano, Ryota Kojima, Ma Teng, and Yasuo Kimura <i>Tohoku University (Japan)</i>	
Dynamic Characteristics of Neuron Models and Microchip Integration of Active Neural Networks	22
Koji Nakajima <i>Tohoku University (Japan)</i>	
Ionic Liquid-Gated Organic Field-Effect Transistors	23
Shohei Iino, Yasuo Kimura and Michio Niwano <i>Tohoku University (Japan)</i>	
UV Excimer laser treatment of SiGe and SiGeSn: Numerical modeling through finite elements methods	24
Stefan Stefanov, Carlos Conde, Elena Martín, Julia Serra, Pio González, Stefano Chiussi <i>New Materials Group, University of Vigo (Spain)</i>	
Ion doped apatite coatings by laser ablation.....	25
Cosme Rodríguez-Valencia, Miriam López-Alvarez, Diego Cordero, Helio Aguiar, Julia Serra, Stefano Chiussi, Pío González <i>New Materials Group, University of Vigo (Spain)</i>	
Innovative porous SiC ceramics from natural precursors	27
Miriam López-Alvarez, Cosme Rodríguez-Valencia, Stefano Chiussi, Julia Serra, Pío González <i>New Materials Group, University of Vigo (Spain)</i>	

Index of Authors

Benedetti, A.	17,18
Bernardy, P.	15
Aguiar, H.	25
Boutinguiza, M.	3
Buca, D.	15
Chiussi, S.	1, 17, 18, 24, 25, 27
Comesaña, R.	3
Conde, C.	18, 24
Cordero, D.	25
Del Val, J.	3
González, P.	1, 24, 25, 27
Grützmacher, D.	15
Holländer, B.	15
Iino, S.	23
Ikeda, M.	7
Kimura, S.	20
Kimura, Y.	20, 21, 23
Kojima, R.	20, 21
Kozłowski, G.	11
Kurps, R.	11
Leitao, J.	9
López-Álvarez, M.	25, 27
Lusquiños, F.	3
Makihara, K.	7
Mantl, S.	15
Martín, E.	24
Miyazaki, S.	7

Murota, J.	5
Nakajima, K.	22
Nakatsuka, O.	13
Niwano, M.	20, 21, 23
Pou, J.	3
Quintero, F.	3
Riveiro, A.	3
Rodríguez-Valencia, C.	25, 27
Sakashita, M.	13
Sakuraba, M.	5
Serra, C.	18
Serra, J.	1, 24, 25, 27
Stefanov, S.	17, 18, 24
Stoica, T.	15
Takeuchi, W.	13
Taoka, N.	13
Teng, M.	21
Tiedemann, A. T.	15
Tillack, B.	11
Wirths, S.	15
Yamamoto, Y.	11
Zaima, S.	13
Zaumseil, P.	11

Index of Institutions

Germany

<i>Forschungszentrum Jülich</i>	15
<i>IHP, Frankfurt an der Oder</i>	11
<i>Technische Universität Berlin</i>	11

Japan

<i>Hiroshima University</i>	7
<i>Nagoya University</i>	7, 13
<i>Tohoku University</i>	5, 20, 21, 22, 23

Portugal

<i>Departamento de Física & I3N, University of Aveiro</i>	9
---	---

Spain

<i>Applied Physics Dpt.</i>	25, 27
<i>CACTI, University of Vigo</i>	17, 18
<i>Industrial Applications of Lasers Group, University of Vigo</i>	1
<i>New Materials Group, University of Vigo</i>	1, 17, 18, 24

General information on research lines of possible interest at the

Laser group of the University of Vigo

Stefano Chiussi, Pio González, Julia Serra

New Material Group, University of Vigo (Spain)

Since the fabrication of the first lasers around 50 years ago, a large variety of improved laser systems delivering laser radiation with wavelength from deep ultra violet (UV) to far infra red (IR) have been developed. Radiation can nowadays be applied to materials continuously or with short pulses of down to few femtoseconds duration and applications are nowadays focused both to R&D and commercial issues, satisfying a wide range of purposes in military, scientific, medical and uncountable industrial fields. The exigencies of the scientific community to exceed detection limits in the analysis of material properties and to deliver photons with extraordinary accuracy in terms of photon energy, spatial coherence and power, together with the industrial demand of having cheap, high power equipments that are reliable and easily to maintain have boosted the improvement of commercial laser systems.

The mission of the “Laser group” at the University of Vigo with its 3 sub-divisions “Industrial applications of Lasers Group”, “Metrology Group” and “New Materials Group” is focused on the development of production and detection processes based on commercial laser systems. This introduction with very general information on the main research lines of the laser group will anticipate extensive lab visits, where infrastructure, basic concepts and recent achievements of different laser assisted processing techniques, such as Laser induced CVD (LCVD), Pulsed Laser Deposition (PLD), Surface functionalization, Excimer Laser Assisted Annealing (ELA) and Crystallization (ELC), Pulsed Laser Induced Epitaxy (PLIE), Laser cleaning, Laser cladding, Laser spinning, Welding, cutting and drilling, as well as TV holography and interferometry will be shown in detail.

Such material processing must inevitably be accompanied by and receive back-up from exhaustive characterization of surfaces and interfaces as well as by fundamental studies of the interactions between laser radiation and the irradiated materials. An overview of the facilities, available in the groups laboratories as well as at the central facilities of the University of Vigo, will be also given introduce the corresponding lab visits with practical demonstrations of the available techniques.

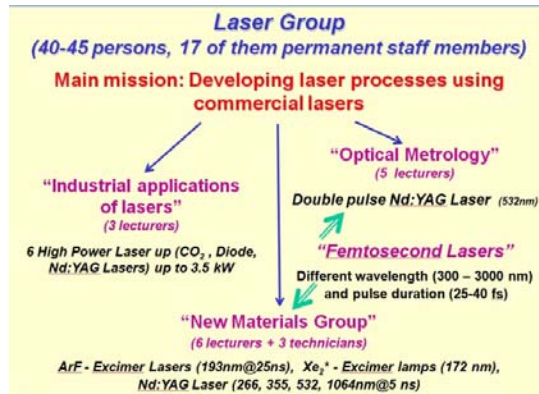


Fig.1 Laser group at UVigo and equipments



Fig.2 Some research topics of the "Industrial applications of lasers" group



Fig.3 Some research topics of the "Metrology" group



Fig.4 Some research topics of the "New Materials" group

LASER PROCESSING AND SYNTHESIS OF MATERIALS AT MICRO- AND NANOSCALE

J. Pou, F. Lusquiños, F. Quintero, M. Boutinguiza, R. Comesaña, A. Riveiro, A. del Val

Department of Applied Physics, EEI, Universidad de Vigo, 36310 – Vigo (Spain);

The successful application of laser technologies to process a broad diversity of materials can only be understood after the recent development of a likewise broad range of laser sources. Thus, the selection of the laser wavelength, laser pulse energy and duration is a key factor for the development of new processing techniques. Figure 1 enumerates the laser techniques in relation to laser-material interaction time.

These laser based techniques can be classified in different groups as a function of their objective. Hence, there are techniques whose purpose is the production of a coating onto a substrate, such as the Pulsed Laser Deposition (PLD) and laser cladding. Our innovations in the field of these techniques start with the production of biocompatible coatings such as hydroxyapatite or bioactive glasses onto metal substrates for implants. More recently, the capabilities of laser cladding have been stretched with our development of an unique facility for microcladding. Laser microcladding of metallic alloys onto metals and copper onto crystalline silicon are some examples of the potential of this technique.

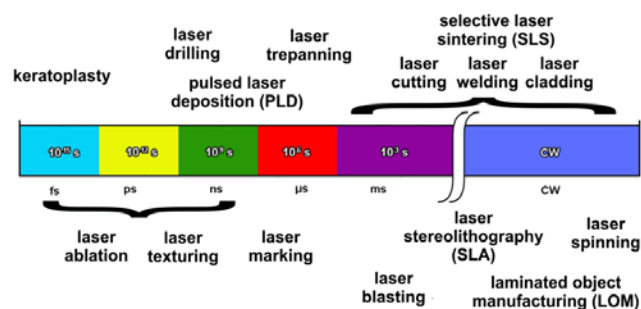


Fig 1. Laser assisted processes as a function of pulse duration.

On the other hand, we have available laser based techniques related to surface modification of materials, such as laser marking, laser texturing or laser blasting. The main purpose of laser texturing and laser blasting is to change the surface roughness and wettability of materials we stretched. Although recent research covers biocompatible polymers (see figure 2), these techniques have been applied mostly on metallic implants such as titanium and titanium alloys.

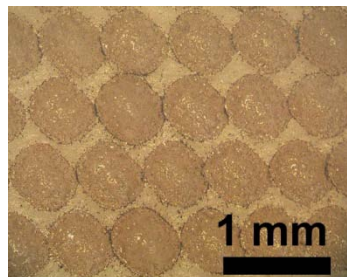


Fig. 2. Laser texturing of PEEK.

Techniques aimed to produce three dimensional structures are classified into additive manufacturing procedures. Here we can include all laser based rapid prototyping techniques such as Selective Laser Sintering (SLS), Laser Stereolithography (SLA), and Laminated Object Manufacturing (LOM).

Referring to the capability of lasers to synthesize nanomaterials, we can highlight two techniques: laser ablation for production of nanoparticles and laser spinning that has been recently introduced for the production of glass nanofibers. TiO_2 nanoparticles with controllable average diameter have been obtained by Continuous Wave (CW) laser ablation of metallic Ti submerged in water. The use of a CW laser contributes to a complete reaction between the metallic species and the evaporated liquid due to long interaction time. Obtained nanoparticles are almost perfect spheres in shape with a stoichiometric composition corresponding to TiO_2 . Furthermore, this technique has been probed to produce hydroxyapatite nanoparticles by laser ablation in ambient conditions. Figure 3.a shows a sample of these hydroxyapatite nanoparticles, while figure 3.b shows the titanium oxide nanoparticles.

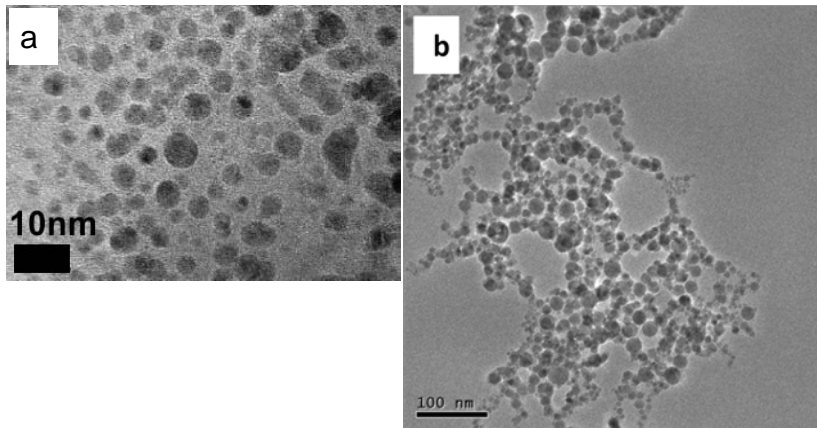


Fig. 3. TEM micrographs showing a) HA and b) TiO₂ nanoparticles produced by laser ablation.

Laser spinning is a new technique which allows the production of ultralong glass nanofibers. This technique opens up new possibilities to produce glass nanofibers that have not been obtained with other methods. Figure 4 shows 45S5 Bioglass® nanofibers produced by Laser spinning. This bioactive glass nanofibers can be employed to build scaffolds for tissue engineering. Additionally, their application for bone defect filling is advantageous compared to granules, thanks to their high length, flexibility and mechanical resistance which make possible to adapt them to any form and insert or remove easily. Also, nanofibers of different functional compositions such as aluminosilicates for refractory applications or lithium silicates for carbon capture have been produced.

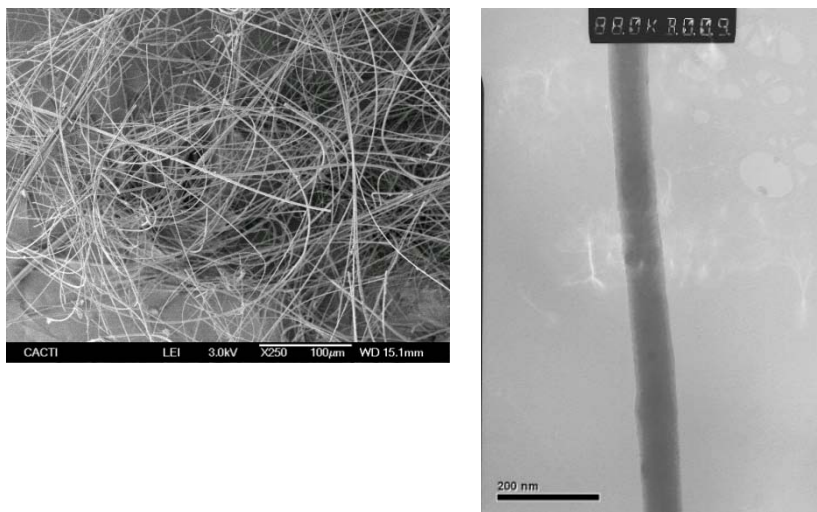


Fig. 4. SEM and TEM micrographs showing and overall view and a detail of the micro- and nanofibers of 45S5 Bioglass® produced by Laser spinning.

In summary, lasers are available today to treat, process, or synthesise many micro- and nanomaterials, opening a broad field of possibilities worth to be explored and applied.

Atomically Controlled Formation of Strained $\text{Si}_{1-x}\text{Ge}_x/\text{Si}$ Quantum Heterostructure for Room-Temperature Resonant Tunneling Diode

Masao Sakuraba* and Junichi Murota

Laboratory for Nanoelectronics and Spintronics,
Research Institute of Electrical Communication, Tohoku University
2-1-1 Katahira, Aoba-ku, Sendai 980-8577, Japan

* Tel: +81-22-217-5549, Fax: +81-22-217-6103, E-mail: sakuraba.masao@myad.jp

High-quality quantum heterostructure of group IV semiconductors such as nanometer-order thick strained $\text{Si}_{1-x}\text{Ge}_x/\text{Si}$ has enabled room-temperature resonant tunneling diode (RTD) [1], and it is important for integration of specified applications, e.g. high frequency oscillation or high speed switching into Si LSIs. In order to improve the RTD performance at room temperature, not only by high quality of heterostructure [2], increase of Ge fraction (i.e. strain and band discontinuity) in the heterostructure is one of the effective ways. In this work, p-type RTD with Si/strained $\text{Si}_{1-x}\text{Ge}_x/\text{Si}(100)$ heterostructure has been investigated [1-4], and it has been demonstrated that introduction of high-Ge-fraction ultrathin $\text{Si}_{1-x}\text{Ge}_x$ layers with atomic-order flat heterointerfaces is effective to improve negative differential conductance (NDC) characteristics at room temperature (**Fig. 1**). Additionally, hole tunneling properties through nanometer order thick Si barriers have been also investigated to explore possibility to overcome limitations of the present materials and structures.

B-doped and undoped strained $\text{Si}_{1-x}\text{Ge}_x/\text{Si}$ heterostructures were epitaxially grown on Si(100) in a SiH_4 (or Si_2H_6)- GeH_4 -(B_2H_6)- H_2 gas mixture using an ultraclean hot-wall low-pressure CVD system [5]. Because total $\text{Si}_{1-x}\text{Ge}_x$ thickness is estimated to be within critical thickness, crystallinity degradation can be avoided. This is essential for uniformity and reproducibility in manufacturing. Especially to suppress the roughness generation at heterointerfaces for higher Ge fraction, Si barriers were deposited at a lower temperature of 400 °C with Si_2H_6 (instead of conventional SiH_4) after the $\text{Si}_{0.42}\text{Ge}_{0.58}$ growth. By this deposition condition, the roughness generation at heterointerfaces (as well as surface) can be effectively suppressed compared with the case of SiH_4 reaction at 500 °C [1].

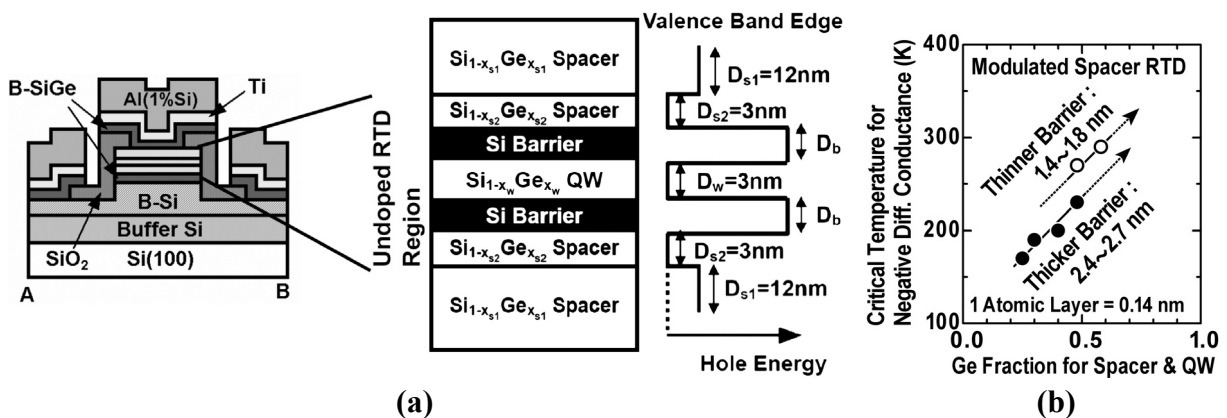


Fig. 1. (a) Schematic RTD structure and expected band alignment for holes. Ge fraction of quantum well and modulated spacers is 0.58. (b) Modulated-spacer Ge fraction (x_{s2}) dependence of critical temperature for NDC for various RTDs ($D_b=1.4\text{--}2.7$ nm).

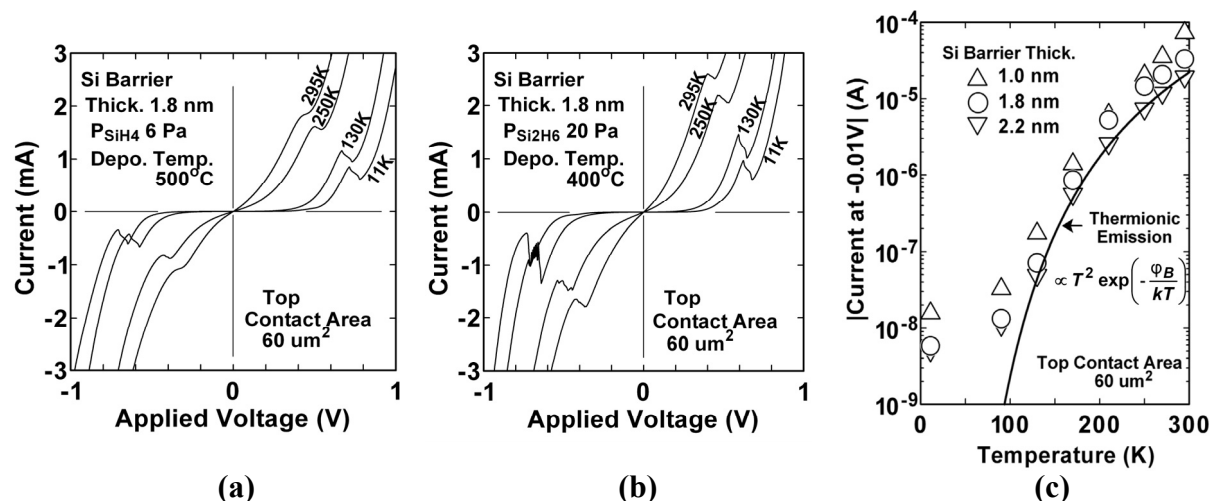


Fig. 2. (a) Current-voltage characteristics of RTDs with 1.8 nm-thick Si barriers for various measurement temperatures. Si barrier growth was performed by reaction of (a) SiH₄ at 500 °C and (b) Si₂H₆ at 400 °C. (c) Temperature dependence of non-resonance current (at -0.01V) for the RTDs with 1.0, 1.8 and 2.2 nm-thick Si barriers. Calculated fitting values based on thermionic-emission are also shown by a solid line. ϕ_B , k and T in the equation are effective barrier height, Boltzmann constant and temperature, respectively.

As shown in current-voltage characteristics of RTDs (**Fig. 2 (a),(b)**), it has been clarified that lowering the Si barrier growth temperature down to 400 °C enables to achieve improved NDC characteristics at around room temperature. Temperature dependence of the non-resonance current shows existence of non-thermal leakage current (observed at lower temperatures below 100 K) and the current tends to increase with decrease of Si barrier thickness. It is concluded that improvement in heterointerface flatness is necessary for the NDC enhancement in nanometer-order thin Si barrier RTD. Additionally, thermionic-emission dominant region (observed at higher temperatures above 100 K in **Fig. 2 (c)**) indicates a possibility that introduction of larger barrier height (i.e. larger band discontinuity) enhances the NDC at room temperature by suppression of thermionic-emission current. The thickness dependence indicates that thermionic-emission current is sensitive to the nanometer-order Si barrier thickness. Therefore, it is confirmed that suppression of roughness generation is indispensable for high reproducibility of the resonant tunneling diodes.

From these results, it is found that only about 1 nm thick Si layer acts as barrier for RTD and there is a possibility that heavy atomic-layer doping of impurity (e.g. C, N and so on) might strongly influence barrier properties for resonant tunneling. Therefore, low-temperature epitaxial growth process (e.g. extremely low-temperature thermal CVD and low-energy plasma CVD [6]) becomes increasingly important to modulate electronic properties of nanometer-order ultrathin layers of group IV semiconductor far from thermal equilibrium.

References

- [1] K. Takahashi, M. Sakuraba and J. Murota, *Solid-State Electron.*, **60** (2011) 112.
- [2] R. Ito, M. Sakuraba and J. Murota, *Semicond. Sci. Technol.*, **22** (2007) S38.
- [3] M. Sakuraba, R. Ito, T. Seo and J. Murota, *ECS Symp. E9: ULSI Process Integration 5, USA, Oct. 7-12, 2007, Abst.No.1283: ECS Trans.*, **11** (2007) 131.
- [4] T. Seo, K. Takahashi, M. Sakuraba and J. Murota, *Solid-State Electron.*, **53** (2009) 912.
- [5] J. Murota, M. Sakuraba and B. Tillack, *Jpn. J. Appl. Phys.*, **45** (2006) 6767.
- [6] M. Sakuraba, K. Sugawara and J. Murota, *Key Engineering Materials*, **470** (2011) 98.

Charge Storage and Optoelectronic Response of Silicide-Nanodots/Si-Quantum-Dots Hybrid-Floating-Gate MOS Devices

Seiichi Miyazaki, Katsunori Makihara, [†]Mitsuhisa Ikeda

Department of Electrical Engineering and Computer Science,
Graduate School of Engineering, Nagoya University,
Furo-cho, Chikusa-ku, Nagoya, 464-8603, Japan

Phone: +81-52-789-3588, E-mail semiya@nuee.nagoya-u.ac.jp

[†]Graduate School of Advanced Sciences of Matter, Hiroshima University,
1-3-1 Kagamiyama, Higashi-Hiroshima, 739-8530, Japan

The application of silicon quantum dots (Si-QDs) and metallic nanodots (NDs) to a floating gate (FG) in MOS devices has attracted much attention because of their potential advantages over conventional FG MOS memories. In fact, multi-valued memory capability can be provided by discrete charged states of Si-QDs originating from the quantum confinement energy as demonstrated in a unique stepwise shift in the threshold voltage of MOSFETs with a Si-QDs floating gate [1-4]. On the other hand, enlarged and stabilized memory window can be achieved by a FG made of metallic NDs with an appropriate work function to form a deep potential well [5, 6]. Recently, we have proposed and fabricated hybrid stacked structures consisting of metallic NDs, Si-QDs and ultrathin interlayer SiO₂ to satisfy both multiple valued capability and charge storage capacity for a sufficient memory window and to open up novel functionality [7]. As for the functionality of such a hybrid nanodots FG, with near-infrared light irradiation, we have verified optical responses caused by transfer of photo-excited electrons from metallic NDs to Si-QDs [8].

Hybrid stacked structures consisting of NiSi-NDs, ultrathin interlayer SiO₂ and Si-QDs were fabricated through the following process sequence. Hemispherical Si-QDs were firstly formed on an ultra-thin thermally-grown SiO₂ by controlling the early stages of LPCVD of pure SiH₄ at 580°C. The areal dot density and the average dot size evaluated by AFM measurements were typically ~5nm and ~3.5x10¹¹cm⁻², respectively. And then, the Si-QDs surface was slightly oxidized in O₂ at 850°C, and followed by SiO₂ deposition from inductively-coupled remote plasma (ICRP) of SiH₄ and excited O₂/Ar at 350°C to obtain the designed thickness. Subsequently, to form NiSi-NDs, Si-QDs were grown again under the same conditions as the first formation of Si-QDs, and the surface was covered uniformly with a ~1.8nm-thick Ni layer by electron beam evaporation and successively exposed to remote H₂ plasma without external heating to enhance surface migration of Ni atoms and full-silicidation of Si-QDs. The 3rd formation of Si-QDs was preformed after ICRP-CVD of ultrathin SiO₂ on NiSi-NDs. Lastly, the top control oxide with a thickness of ~20nm, Al gates with a diameter of 1 mm and Al back contact with a window for light irradiation were sequentially fabricated to complete hybrid FG MOS structures (Fig. 1).

High-frequency capacitance-voltage (C-V) characteristics of the MOS capacitor with the hybrid FG show positive and negative flat-band voltage shifts depending on the polarity and the maximum magnitude of applied gate bias (Fig. 2), and confirm stable charge storage in a deep potential well in each of NiSi-NDs. Considering that electrons in NiSi-NDs can be

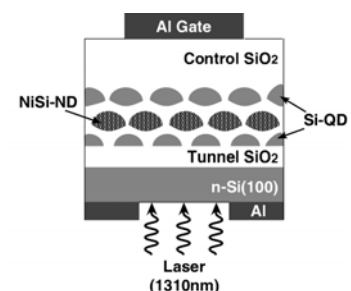


Fig. 1 Schematic of a MOS capacitor with a NiSi-NDs/Si-QDs hybrid FG.

excited by irradiation of infrared light of being not absorbed in the Si substrate and Si-QDs, such an infrared light irradiation can cause electron transfer from NiSi-NDs to Si-QDs selectively (Fig. 3) and induces flat-band voltage shift as a result of the change in the charge centre in the hybride FG. To investigate the response of photoexcited electrons in the hybrid FG stack to the change of gate bias, the transient current induced by pulsed gate voltages was evaluated by connecting the MOS capacitor with a 1 kΩ resistance in series and measuring the voltage drop across it with a lock-in amplifier. As shown in Fig. 4, a distinct change in the output voltage (V_{OUT}) of the lock-in amplifier was detected in synchronized timing of the infrared light irradiation under the application of periodic pulsed gate voltage. This result can be attributed to an increase in the displacement current mainly due to the photoexcited electron transfer from the NiSi-NDs to the top and bottom Si-QDs in response to pulsed gate voltage. Namely, the difference in V_{OUT} (ΔV_{OUT}) between in the dark and under light irradiation corresponds to the amount of charge transferred from the NiSi-NDs to the Si-QDs. The ΔV_{OUT} measured in each bias polarity as a function of pulse voltage is summarized in Fig. 5. The ΔV_{FB} almost linearly increased with pulse voltage over $\pm 2.0V$. This result indicates that the amount of transferred charge in each cycle is limited to a certain level determined by gate voltage and the signals proportional to gate voltage are associated with charging and discharging a capacitor as long as the photoexcited electron transfer can respond to pulsed gate voltage.

Acknowledgments

This work was supported in part by Grants-in Aid for Scientific Research (A) No. 24246054 from the Ministry of Education, Culture, Sports, Science and Technology, Japan. In addition, the author deeply appreciates that MOSFETs with hybrid NDs FG were fabricated successfully by utilizing the clean room facilities of Research Institute for Nanodevice and Bio Systems (RNBS), Hiroshima Univ.

References

- [1] S. Tiwari et al., *Appl. Phys. Lett.*, vol. 68, pp. 1377-1379, 1996. [2] A. Kohno et al., *Jpn. J. Appl. Phys.* 2, Lett., vol. 40, pp. L721-L723, 2001. [3] M. Ikeda, et al., *Jpn. J. Appl. Phys.*, vol. 42, pp. 4134-4137, 2003. [4] R. Matsumoto, et al. *Jpn. J. Appl. Phys.*, vol. 47, pp. 3103-3106, 2008. [5] P. H. Yen et al., *Appl. Phys. Lett.*, vol. 87, pp. 193504-1 -193504-3, 2005. [6] K. Shimanoe et al., *IEICE Trans. Electron*, vol. E92-C, pp. 616-619, 2009. [7] S. Miyazaki, et al., *Thin Solid Films*, vol. 518, pp. 530-534, 2010. [8] N. Morisawa, et al., *Jpn. J. Appl. Phys.*, vol. 49, pp. 04DJ04-1-04DJ04-4, 2010.

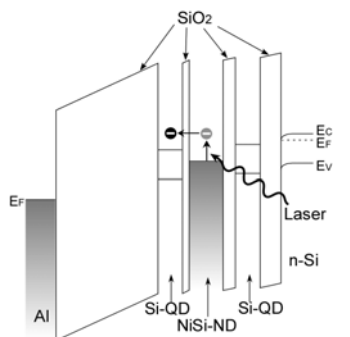


Fig. 3 Energy band diagram of the MOS capacitor with the NiSi-NDs/Si-QDs hybrid floating gate stack in which photoexcited electrons are transferred from the NiSi-NDs to the top Si-QDs with infrared light irradiation.

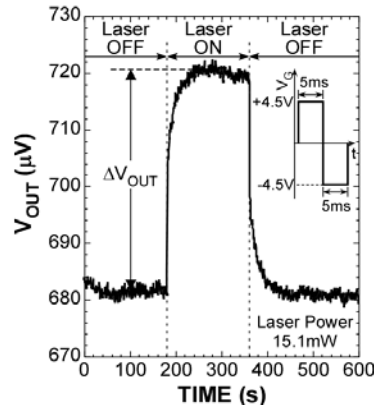


Fig. 4 The response of electrons excited by 1310 nm light irradiation in the NiSi-NDs/Si-QDs hybrid FG to pulsed gate voltage of $\pm 4.5 V$ at a frequency of 100 Hz.

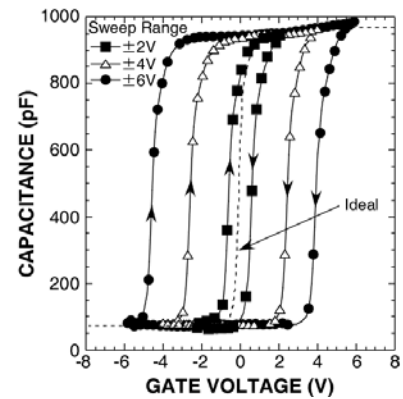


Fig. 2 100 kHz capacitance-voltage (C-V) characteristics of a MOS capacitor with the NiSi-NDs/Si-QDs hybrid FG. The gate voltage sweep rate was set at 100 mV/s. The ideal C-V curve is also shown with a dashed line.

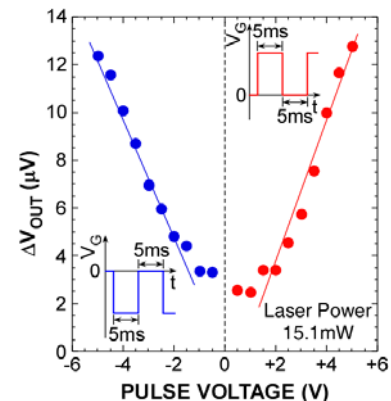


Fig. 5 The response of electrons excited by 1310 nm light irradiation in the NiSi-NDs/Si-QDs hybrid FG to pulsed gate voltage at a frequency of 100 Hz as a function of pulse voltage.

Optical studies of Ge/Si based heterostructures and Si interstitials related defects in SiGe alloys

J. P. Leitão

Departamento de Física and I3N, Universidade de Aveiro
 Campus Universitário de Santiago, 3810-193 Aveiro, Portugal
 Tel: +351 234 370 286, Fax: +351 234 378 197, joaquim.leitao@ua.pt

This work is focused on the application of photoluminescence (PL) for the study of a low dimensional structure based on the Si/Ge system and of Si interstitial related optical centers in Si and SiGe alloys. In the first part, we consider a superlattice structure with embedded Ge islands grown by molecular beam epitaxy (MBE) at 600°C on top of a Si(001) substrate [1]. The samples were irradiated with 2.0 MeV protons to fluences in the range 2×10^{12} - 2×10^{14} cm⁻². The structural and optical properties of the samples were investigated by cross-sectional transmission electron microscopy, X-ray reciprocal space mapping (RSM), X-ray reflection (XRR) and Rutherford backscattering/channeling. No changes to the as-grown heterostructure were observed after the irradiation in all fluences (Fig. 1). The nominal period of the superlattice was confirmed. The radiative recombination related to type-II transitions in the Si/Ge interface was observed in PL measurements additional to free and bound excitons recombination in the Si layers and substrate, near the energy band gap of Si. The PL related to the Ge islands was observed even for the highest irradiation fluence showing an extremely high radiation hardness of the studied structure, which was confirmed by the absence of changes in the structural properties (Fig. 1).

In the second part of the work, the Si interstitial related W and X centers, were studied by photoluminescence and the results compared with the ones from first-principles calculations [2]. The samples were obtained after the growth of a Si or Si_{1-x}Ge_x alloy layers (x=0.0069, 0.0125) on top of a Si(001) substrate at 800°C by MBE. For the production of the centers, irradiation with 875 keV protons (dose of 10^{16} H⁺ cm⁻²) followed by annealing of 15 min, in N₂ atmosphere, at a temperature in the range 100 – 650°C, was performed. It was found that the annealing temperature (300°C) that maximizes the PL intensity of the W center is independent of the Ge content, whereas for the X center, a shift was observed from the Si layer (400°C) to the SiGe alloys (450°C) suggesting that the minority Ge atoms delay the formation of this center. The radiative excited state in both centers comprises a pseudodonor state, where a trapped exciton combines a tightly bound hole and a diffuse electron. No acceptor level in the gap was found for either of the centers. The ionization energies of both centers were calculated from a temperature dependence of the PL intensity and the hole binding energy was extracted considering also the spectroscopic energy of the W and X lines in the spectra. The calculated change rates of donor levels with Ge content are in qualitative agreement with the hole binding energy shifts obtained from the experiments. Our results support the previous assignment of the trigonal (I₃) and tetragonal (I₄) forms of tri- and tetra-interstitial defects to the W and X centers, respectively.

[1] A. Fonseca, N. A. Sobolev, J. P. Leitão, E. Alves, M. C. Carmo, N. D. Zakharov, P. Werner, A. A. Tonkikh and G. E. Cirlin, *J. Luminescence* 121, 417 (2006)

[2] J. P. Leitão, A. Carvalho, J. Coutinho, R. N. Pereira, N. M. Santos, A. O. Ankiewicz, N. A. Sobolev, M. Barroso, J. Lundsgaard Hansen, A. Nylandsted Larsen and P. R. Briddon, *Phys. Rev. B* 84, 165211 (2011)

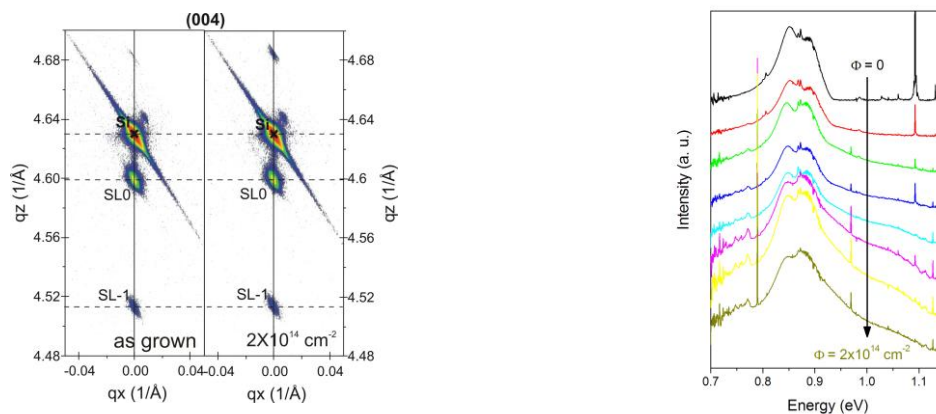


Fig. 1 a) X-ray reciprocal space map for the as-grown and irradiated to the highest fluence samples. The Si substrate and superlattice related peaks are identified. b) Photoluminescence spectra of as-grown and irradiated samples (range from 2×10^{12} to $2 \times 10^{14} \text{ cm}^{-2}$).

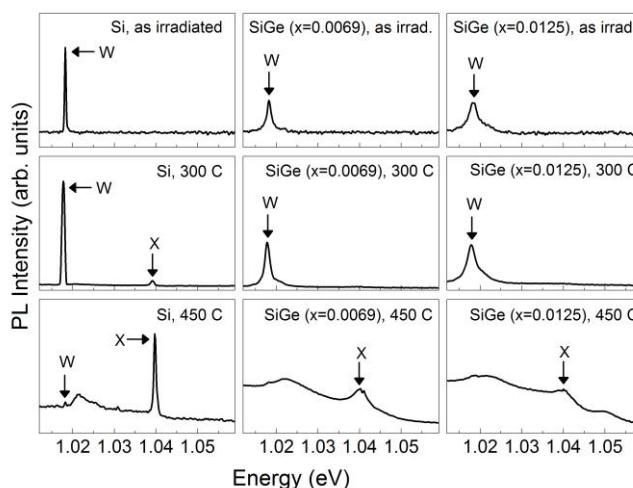


Fig. 2. PL spectra recorded at 5 K for the Si and SiGe layers as irradiated (top row), after an annealing at 300°C (middle row), and after annealing at 450°C (bottom row). Both W and X lines are identified in the spectra.

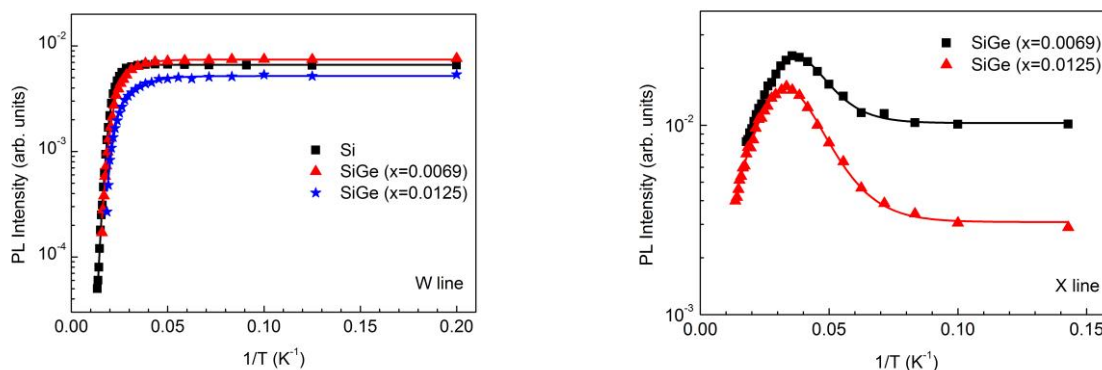


Fig. 3 Integrated PL intensity temperature dependence of the W and X lines in Si (squares) and SiGe alloys with $x=0.0069$, 0.0125 (triangles and stars, respectively). The lines represent the best fit to the experimental points according to the model described in Ref. [2].

Low threading dislocation density Ge growth and heavy phosphorus doping in Ge

Yuji Yamamoto¹⁾, Peter Zaumseil¹⁾, Grzegorz Kozłowski¹⁾, Rainer Kurps¹⁾ and Bernd Tillack^{1,2)}

¹⁾ *IHP, Im Technologiepark 25, 15236 Frankfurt (Oder), Germany*

Tel.: +49-335-56-25-156 Fax: +49-335-56-25-661

E-mail: yamamoto@ihp-microelectronics.com

²⁾ *Technische Universität Berlin, HFT4, Einsteinufer 25, 10587, Berlin, Germany*

Heteroepitaxial growth of Ge on Si has generated great interest for different applications such as optoelectronic devices [1] and novel CMOS technologies [2]. Low threading dislocation density (TDD) is required to prevent degradation of electrical properties of devices, such as dark current of optical detectors. Deposition of Ge on virtual substrate is widely investigated using different approaches to reduce TDD [3-5]. Additionally, N doping such as phosphorus in Ge have been widely investigated because of potential to change Ge to direct band gap material by filling electron into L-valley. In this report, we demonstrate low threading dislocation density Ge growth by combination of cyclic annealing and etching. The heavy P doping in Ge by atomic-layer doping (P-ALD) approach is also discussed.

Epitaxial growth of Ge is carried out using a single wafer reduced pressure CVD system. After HF last clean, the wafer is baked at 850-1000°C and cooled down to 600°C in H₂ and further cooled down to 300°C in N₂ to form hydrogen-free Si surface. Then thin 2-dimensional Ge seed layer (~50 nm) is deposited at 300°C using GeH₄ in N₂ carrier gas. After that the 2nd Ge layer is deposited at 550°C with H₂-GeH₄ gas mixture. For TDD reduction, cyclic annealing [5] in H₂ is performed during the Ge growth. After the deposition, the Ge layers of some samples are etched back by HCl in the CVD reactor for thinning. For the P-ALD experiment, the Ge surface is exposed to PH₃ with N₂ carrier gas. The exposure temperature is varied between 100-300°C. In order to investigate the effect of hydrogen-termination of the Ge surface, some wafers are cooled down in H₂ environment after the Ge layer deposition. After the exposure step the temperature is changed back to 300°C in N₂ and the Ge layer growth is continued with N₂-GeH₄ gas mixture. P dose and profile are measured by SIMS. Active P dose is determined by Hall measurement at 10 K.

TDD as a function of blanket Ge thickness is shown in Fig. 1. In the case of the Ge growth with cyclic annealing (○), TDD is decreasing with increasing Ge thickness and $\sim 7 \times 10^5 \text{ cm}^{-2}$ is achieved for 4.7 μm thick Ge [5]. By 4.5 μm thick Ge deposition and etching process (□), the level of the TDD is lower compared to the TDD of Ge layer of same thickness deposited by cyclic annealing process. For example TDD is reduced to $\sim 1.3 \times 10^6 \text{ cm}^{-2}$ for a sample which was thinned to 1.8 μm, which is around one order of magnitude lower compared to deposited samples without etching. If the layer is thinned further the TDD is increasing, but is still lower compared to TDD measured for the Ge layers obtained by deposition only.

AFM images of blanket Ge surface before (4.5 μm) and after etching (1.8 μm) are shown in Fig. 2. By etching, cross hatch pattern becomes slightly smeared, but the surface roughness is not increased. Further etching was increasing the surface roughness.

In order to discuss impact of hydrogen-termination on Ge surface, P dose as function of PH₃ exposure temperature is shown in Fig. 3. During the cooling, N₂ or H₂ is chosen as carrier gas. In the case of the sample cooled down in H₂, very few P is adsorbed on the Ge surface at 100°C. With increasing PH₃ exposure temperature adsorbed P dose is increased. On the other hand, in the case of the sample cooled down in N₂, $\sim 8 \times 10^{13} \text{ cm}^{-2}$ of P is adsorbed even at 100°C. In this case, temperature dependence of P dose is small. At 300°C, no clear difference between N₂ and H₂ cooling is observed. These results indicate that the P adsorption is suppressed by hydrogen-termination of the Ge surface in the case of cooling down in H₂. The hydrogen desorption from the Ge surface starts from $\sim 200^\circ\text{C}$ resolving the surface passivation [6].

In Fig. 4, P dose as function of PH₃ exposure time at various PH₃ partial pressures is shown.

The PH₃ exposure is performed at 300°C on hydrogen-free Ge surface. For all PH₃ partial pressure used, P dose is increasing with increasing PH₃ exposure time and saturated at $\sim 1.5 \times 10^{14}$ cm⁻², which value is close to a quarter of monolayer of Ge (100). The saturation value does not depend on PH₃ partial pressure. The incorporated P dose Q_r on the hydrogen-free Ge surface can be described by Langmuir type kinetic.

$$Q_r = N_t \left[1 - \exp \left\{ -k_r \left(\frac{K P_{PH_3}}{1 + K P_{PH_3}} \right) \right\} \right] \quad (1)$$

Where N_t is saturation value of incorporated P dose, k_r and K are reaction rate and thermal equilibrium constants of PH₃ adsorbed on the Ge surface, respectively. Good agreement to Langmuir type adsorption model is obtained with $N_t = 1.55 \times 10^{14}$ cm⁻² (a quarter of monolayer), $k_r = 77$ s⁻¹ and $K = 3.0 \times 10^{-2}$ Pa⁻¹.

References

- [1] J. Murota et al. *Jpn. J. Appl. Phys.* **45** 9A (2006) 6767
- [2] B. Tillack et al. *Appl. Surf. Sci.* **254** (2008) 6013
- [3] Y. Yamamoto et al. *Thin Solid Films* **518** (2010) S44
- [4] G. Scappucci et al. *Phys. Rev. B* **80** (2009) 233202
- [5] Y. Yamamoto et al. *Solid State Electronics* **60** (2011) 2
- [6] J. Y. Lee et al. *J. Chem. Phys.* **118** 4 (2003) 1929

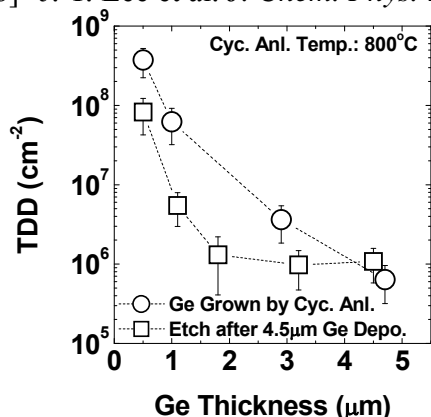


Fig. 1. TDD as function of Ge thickness. Blanket Ge is deposited. (○) shows the Ge sample deposited by cyclic annealing process and (□) shows the sample with Ge deposition (4.5 μm) and etching.

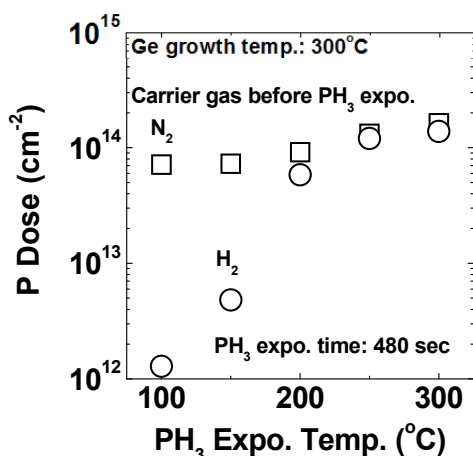


Fig. 3. P dose as function of PH₃ exposure temperature. N₂ (□) or H₂ (○) is used during temperature change before PH₃ exposure. PH₃ exposure time is 480 sec.

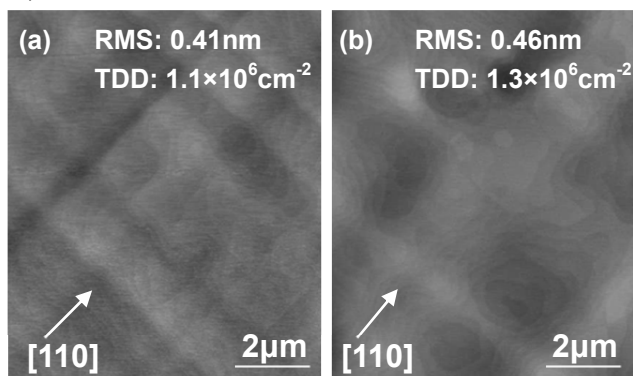


Fig. 2. AFM images of the sample after blanket Ge growth with cyclic annealing (a) and followed by etching (b). Ge thicknesses are (a) 4.5 μm and (b) 1.8 μm, respectively. [110] directions are shown by arrows.

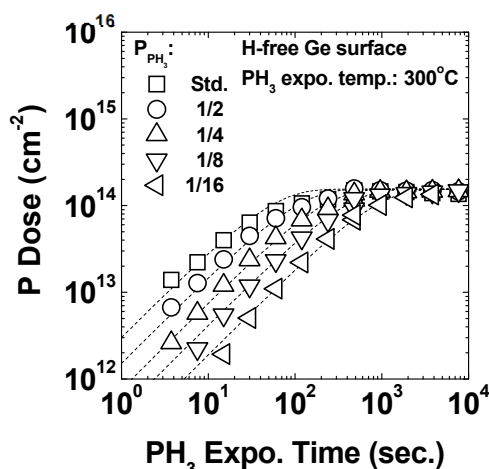


Fig. 4. P dose as function of PH₃ exposure time. PH₃ partial pressure is varied. Dash lines are calculated by using equation (1) with $N_t = 1.55 \times 10^{14}$ cm⁻², $k_r = 77$ s⁻¹ and $K = 3.0 \times 10^{-2}$ Pa⁻¹.

Epitaxial Growth and Characterizations of $\text{Ge}_{1-x}\text{Sn}_x$ and $\text{Ge}_{1-x-y}\text{Si}_x\text{Sn}_y$ Thin Layers for Nanoelectronic and Optoelectronic Applications

Osamu Nakatsuka, Noriyuki Taoka, Mitsuo Sakashita, Wakana Takeuchi, and Shigeaki Zaima
Graduate School of Engineering, Nagoya University
Furo-cho, Chikusa-ku, Nagoya 464-8603, Japan
Tel: +81-51-789-5963, Fax: +81-52-789-2760, E-mail: nakatuka@alice.xtal.nagoya-u.ac.jp

$\text{Ge}_{1-x}\text{Sn}_x$ and $\text{Ge}_{1-x-y}\text{Si}_x\text{Sn}_y$ alloy thin films are attractive for future Si nanoelectronic and optoelectronic applications such as high carrier mobility MOSFET, photo detector, quantum well laser, photovoltaic cell, and so on. We can engineer the energy band diagram and carrier properties with controlling the lattice constant and strain structures of these thin layers. However, the epitaxial growth of group IV-materials including Sn with its content higher than a few % is not so easy, because Ge-Sn and Si-Sn systems are eutectic, and Sn precipitation easily occurs due to the low equilibrium solid solubility of Sn in Ge and Si. We have developed the low temperature growth technique of $\text{Ge}_{1-x}\text{Sn}_x$ and the lattice mismatch engineering between $\text{Ge}_{1-x}\text{Sn}_x$ and various substrates [1-3]. Recently, we achieved the growth of $\text{Ge}_{1-x}\text{Sn}_x$ epitaxial layers with a Sn content as high as 13% and 27% on Ge and InP substrates, respectively [3].

Engineering the electronic and optical properties of $\text{Ge}_{1-x}\text{Sn}_x$ is also essentially important for its applications. Figure 1 shows the Hall concentration in undoped $\text{Ge}_{1-x}\text{Sn}_x$ thin layers grown on Si-on-insulator (SOI) substrates as a function of the Sn content for as-grown, N_2 -annealed, and H_2 -annealed samples [4]. We can generally observe p-type conduction even for an undoped Ge epitaxial layer due to unintentional hole generation from vacancy defects in Ge. We found that the Sn incorporation with the content of 0.1% effectively reduces the Hall carrier concentration. We consider that preferential formation of Sn-vacancy pairs is a key to reduce the concentration of electrically active vacancies. In addition, we found that the H_2 -annealing reduces the Hall carrier concentration of Ge and $\text{Ge}_{1-x}\text{Sn}_x$ thin layers.

We demonstrate the electrical properties at the interface between $\text{Ge}_{1-x}\text{Sn}_x$ and a substrate. We prepared a pn junction with a p^+ -doped $\text{Ge}_{1-x}\text{Sn}_x$ epitaxial layer on n-Ge(001) substrate. Figure 2 shows the current density-voltage characteristics of the p^+ - $\text{Ge}_{1-x}\text{Sn}_x$ /n-Ge junction for various measurement temperatures [5]. We found that the Sn incorporation into Ge does not generate any interfacial defects causing excess leakage current. Instead, the Sn incorporation reduces the leakage current at low temperature below 170K in the reverse bias condition compared to a p^+ -Ge/n-Ge junction sample (*not shown*).

We also examined the epitaxial growth of $\text{Ge}_{1-x-y}\text{Si}_x\text{Sn}_y$ ternary alloys on a Ge substrate [6]. We can deposit a $\text{Ge}_{1-x-y}\text{Si}_x\text{Sn}_y$ epitaxial layer whose lattice constant was controlled to match bulk-Ge. Figure 3 shows the x-ray diffraction two dimensional reciprocal space map (XRD-2DRSM) for a $\text{Ge}_{1-x-y}\text{Si}_x\text{Sn}_y$ layer grown on a Ge(001) substrate. The Si and Sn compositions were determined to be 58% and 15%, respectively, from Raman scattering spectroscopy and Rutherford back scattering methods. We achieved the pseudomorphic growth of $\text{Ge}_{1-x-y}\text{Si}_x\text{Sn}_y$ ternary layer even with a high Sn content, since the strain of this layer to Ge is suppressed as small as 0.5% with local strain compensation between Si and Sn atoms. The full width at half maximum values of the ω rocking curves of pseudomorphic $\text{Ge}_{1-x-y}\text{Si}_x\text{Sn}_y$ layers are as small as that of a Ge substrate, indicating the superior crystalline structures of $\text{Ge}_{1-x-y}\text{Si}_x\text{Sn}_y$ layers. Figure 4 shows the Ge-Si-Sn content dependence of the energy band gap calculated assuming Vegard's law. Ge-Si-Sn ternary alloy realizes the energy bandgap engineering with lattice-matching system on Ge [7]. We expected the energy bandgap of $\text{Ge}_{1-x-y}\text{Si}_x\text{Sn}_y$ controlled to be from 0.66 eV of Ge to as high as 1 eV in this study.

Acknowledgements

This work was partly supported by a Grant-in-Aid for Specially Promoted Research (No. 22000011) from the MEXT and the ALCA Program from JST in Japan.

References

- [1] S. Takeuchi *et al.*, *Semicond. Sci. Tech.* **22**, S231 (2007).
- [2] Y. Shimura *et al.*, *Thin Solid Films* **518**, S2 (2010).
- [3] M Nakamura *et al.*, *Thin Solid Films* **520**, 3201 (2012).
- [4] O. Nakatsuka *et al.*, *Solid-State Electron.* *submitted*.
- [5] S. Asaba *et al.*, in *Abstr. of IUMRS-IECM*, Yokohama, Japan, Sept., 2012, *accepted*.
- [6] T. Yamaha *et al.*, *Electrochem. Soc. Trans.*, *accepted*.
- [7] V. R. D'Costa *et al.*, *Phys. Rev. Lett.* **102**, 107403 (2009).

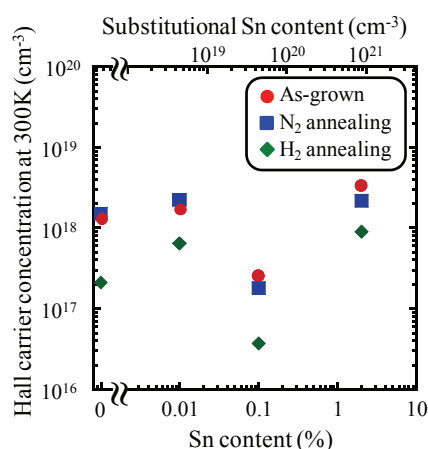


Fig. 1 The Sn content dependence of the Hall concentration in undoped $\text{Ge}_{1-x}\text{Sn}_x$ thin layers grown on SOI substrates for as-grown, N_2 -annealed, and H_2 -annealed samples [4].

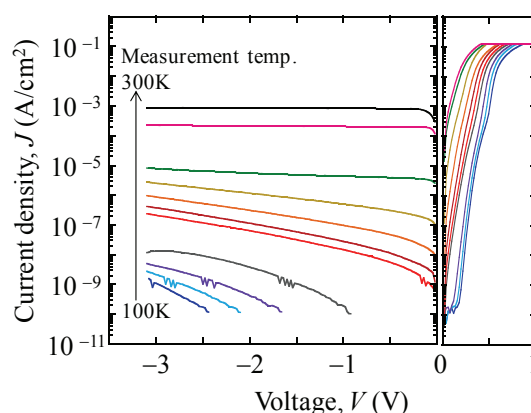


Fig. 2 The current density-voltage characteristics of the $\text{p}^+\text{-Ge}_{1-x}\text{Sn}_x/\text{n-Ge}$ junction for various measurement temperatures.

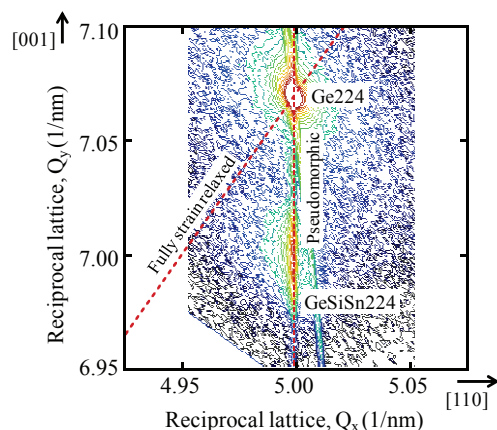


Fig. 3 XRD-2DRSM around the Ge224 Bragg reflection for a $\text{Ge}_{1-x}\text{Si}_x\text{Sn}_y$ epitaxial layer grown on a Ge(001) substrate.

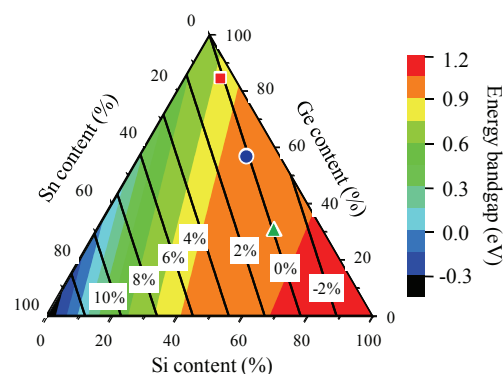


Fig. 4 The Ge-Si-Sn content dependence of the calculated energy bandgap. The solid lines with percentages correspond to the lattice mismatch for bulk-Ge. Some symbols indicate the content conditions of samples prepared in our study.

Epitaxial Growth of $\text{Ge}_{1-x}\text{Sn}_x$ with high Sn content by Reduced Pressure CVD

S. Wirths, D. Buca, A. T. Tiedemann, B. Holländer, P. Bernardy, T. Stoica, D. Grützmacher,
and S. Mantl

PGI9-IT, Forschungszentrum Jülich (Germany)

The most promising route towards photonic integrated circuits on Si relies on the development of appropriate group IV semiconductors, such as (Si)GeSn alloys. At high Sn contents these alloys present a direct energy band-gap [1] which is the requirement for efficient light emitters and detectors. Moreover, (Si)GeSn layers may act as buffer layers to introduce tensile strain in Ge [2] for high mobility channels of high performance MOSFETs. However, synthesizing these alloys is very challenging, because of the low solid solubility of Sn in Ge of about 1 at.%.

We are investigating epitaxial $\text{Ge}_{1-x}\text{Sn}_x$ layers grown by low temperature Reduced Pressure CVD using an AIXTRON Tricent® cold wall system with a showerhead technology [3]. Ge_2H_6 and SnCl_4 are employed as Ge and Sn precursors and N_2 as carrier gas. At a reactor pressure of 60 mbar the $\text{Ge}_{1-x}\text{Sn}_x$ layers were grown at susceptor temperatures between 375 - 475°C. The layers were studied by Rutherford Backscattering/Channeling (RBS/C) and Transmission Electron Microscopy (TEM) to analyze the layer stoichiometry, thicknesses and crystal quality. XRD measurements and Raman spectroscopy are employed to measure the strain status of the structures.

$\text{Ge}_{1-x}\text{Sn}_x$ layers were grown on Si(100) substrates and Ge buffer layers at different growth temperatures and Sn precursor fluxes in order to investigate GeSn growth properties on different substrates. In Fig. 1(a) the Sn concentration, measured by RBS, is shown as a function of the partial pressure ratio of Ge_2H_6 and SnCl_4 for layers grown at 475°C on Si(100). It is found, that decreasing the partial pressure ratio the Sn concentration increases from 1.8 % to about 18 %. However, SEM and RBS analysis reveal Sn segregation at these growth conditions for $x > 1.8$ %. Using this optimized partial pressure ratio and decreasing the growth temperature to 375°C single crystalline layers with Sn concentration up to 10 % were grown (Fig.1b). Minimum yield values χ_{\min} of 20 % prove a substitutional fraction of Sn atoms of about 80 %. The GeSn growth is significantly improved in terms of crystal quality and surface roughness using Ge buffered Si(100) substrates. Figure 2(a) shows RBS random and aligned spectra of a partially relaxed 195 nm thick $\text{Ge}_{0.925}\text{Sn}_{0.075}$ layer grown on a Ge buffer layer. Both, high crystal quality and a high substitutionality of Sn > 90 % are proved by a χ_{\min} of 6 %. Raman spectra for three $\text{Ge}_{0.925}\text{Sn}_{0.075}$ layers with thicknesses of 30 nm, 90 nm and 195 nm are presented in Fig. 2b. As a reference for the Ge-Ge modes a spectrum of Ge bulk sample is shown in black. The Raman shift towards lower wavenumbers for increasing layer thickness is due to the strain relaxation. This is confirmed by the TEM image in Fig. 3. For the partially relaxed $\text{Ge}_{0.925}\text{Sn}_{0.075}$ layer dislocations are visible at the GeSn/Ge interface. FWHM values of about 4 cm^{-1} indicate high crystal quality. Moreover, the TEM image of the 30 nm thick $\text{Ge}_{0.925}\text{Sn}_{0.075}$ layer (Fig. 3) shows no dislocations at the GeSn/Ge interface, indicating pseudomorphic GeSn growth on Ge(100).

References

- [1] P. Moontragoon *et al.*, Semicond. Sci. Technol. **22**, 742 (2007)
- [2] Y.-Y. Fang *et al.*, Applied Physics Letters **90**, 061915 (2007)
- [3] S. Wirths *et al.*, Proceeding of the 6th International SiGe Technology and Device Meeting, 4-6 June 2012 Berkeley, 7 (2012)

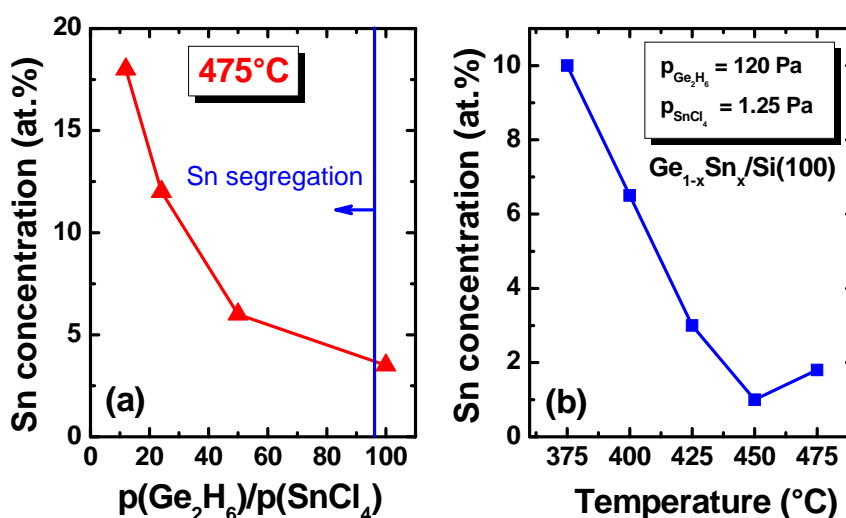


Fig. 1 (a) Sn concentration as a function of the partial pressure ratio of Ge_2H_6 and SnCl_4 grown at 475°C on $\text{Si}(100)$. For smaller ratios, strong Sn segregation is observed. (b) Sn concentration as a function of growth temperature at a fixed partial pressure ratio.

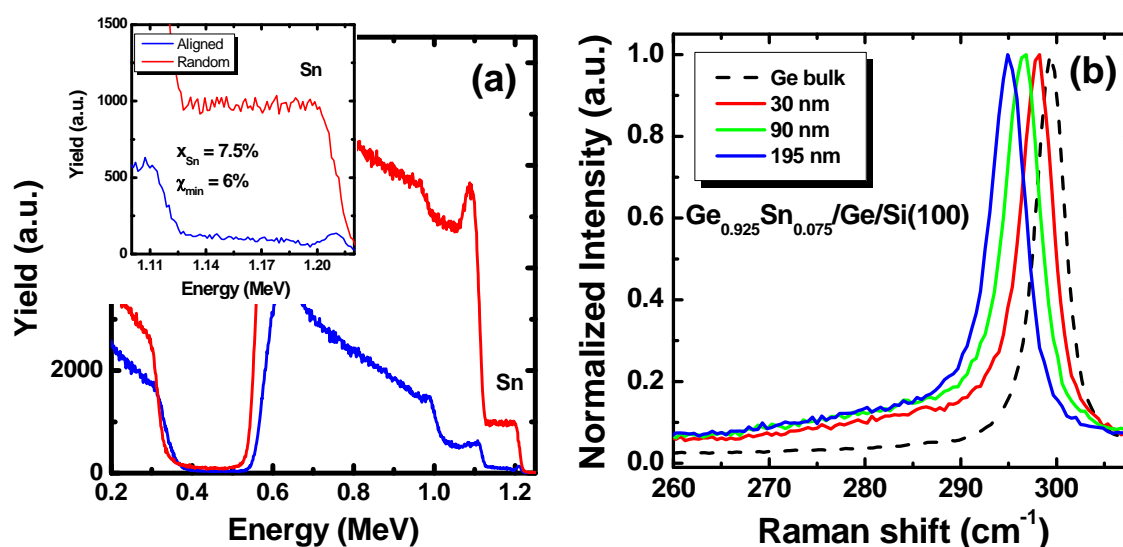


Fig. 2 (a) Rutherford Backscattering (RBS) random (red) and aligned spectra and (b) Raman modes for three $\text{Ge}_{0.925}\text{Sn}_{0.075}$ layers grown on a 600 nm thick Ge buffer layer.

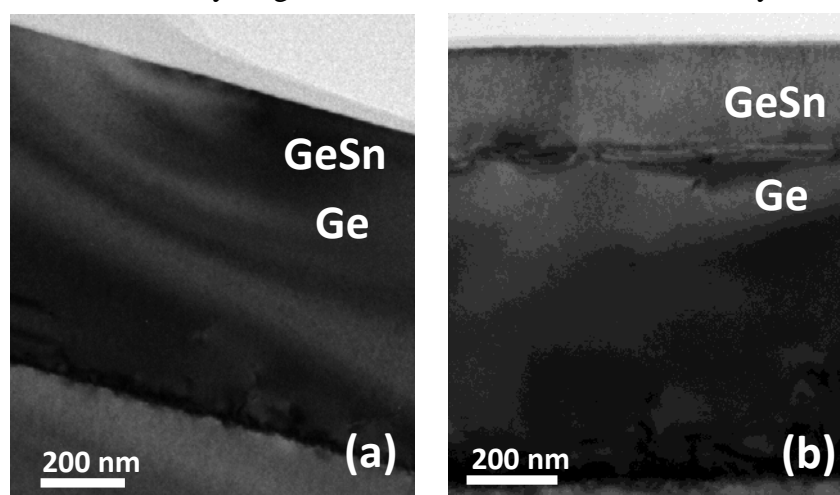


Fig. 3 TEM images of a (a) fully strained 30 nm thick $\text{Ge}_{0.925}\text{Sn}_{0.075}$ layer and a (b) relaxed 195 nm thick $\text{Ge}_{0.925}\text{Sn}_{0.075}$ layer grown on a Ge buffer layer.

FIB preparation and TEM characterisation of Si/Sn alloys

Alessandro Benedetti, *Stefan Stefanov, *Stefano Chiussi

CACTI, University of Vigo, *New Materials Group, University of Vigo, Vigo (Spain)

GeSn and SiGeSn alloys represents one of the most attractive group IV semiconductor materials, due to the higher carrier mobility they can achieve¹.

It is therefore of paramount importance to be able to characterise them in terms of morphology, composition, cristallinity and strain distribution with a spatial resolution within the nanometre range. This can be nowadays routinely performed by Trasmision Electron Microscopy (TEM), but the specimen requirements for a successful TEM analysis are stringent: the sample has to be electron transparent, as little amorphised as possible and free from local thickness variations.

Focused Ion Beam (FIB) is a well known technique based on the use of a Ga⁺ beam, capable of preparing thin TEM-ready lamellas from the region of interest, with a nanometre scale precision. However, in order to minimise the amorphisation of both the sides and the top of the thin lamella the ion currents have to be carefully chosen, depending on the electrical and mechanical characteristics of the analysed material.

GeSn alloys in particular are very sensitive to the ion beam, due to the instability of the cubic structure of α -Sn and the low thermodynamic solubility of Sn in Ge (<1%)²

In this work, we briefly summarise the theoretical and practical aspects of the tecnique, discussing the main problems encountered and any possible solution. Various experimental results from GeSn specimens are also presented, proving that the FIB technique can not only provide suitable samples for High Resolution TEM analysis (Fig. 1 left) but also yield valuable information on the Sn distribution (Fig. 1 right).

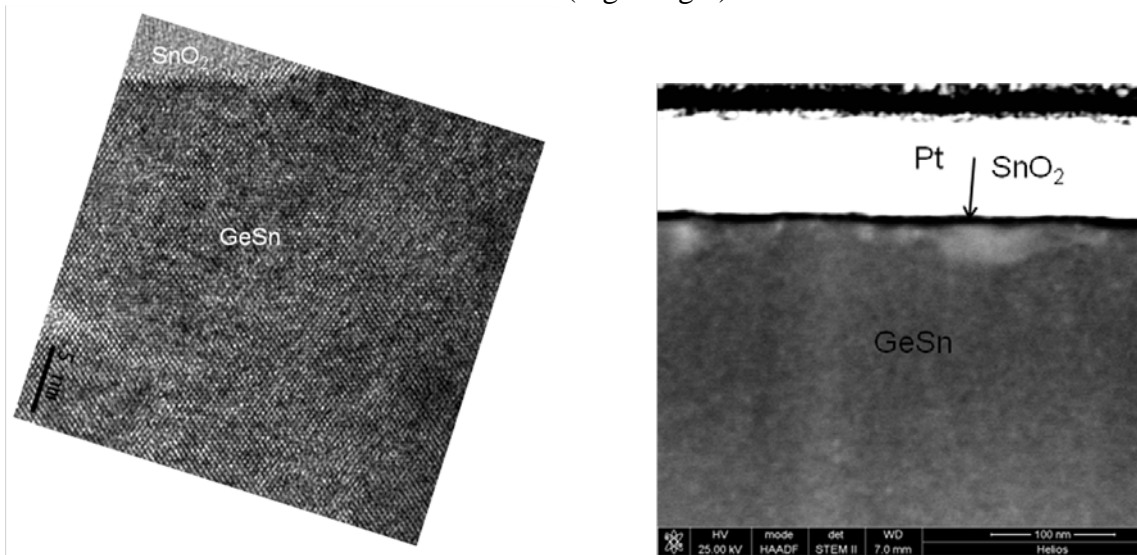


Fig. 1 HREM image of a GeSn sample, showing good crystallinity and little amorphisation (left); FIB-STEM image of a similar sample, with Sn clusters clearly visible near the GeSn/SnO₂ interface (right).

References

- ² G. Grzybowski et al., App. Physics Letters **99**, 171910 (2011).
¹ D.W. Jenkins et al., Phys. Rev. B **36**, 7994–8000 (1987).

Laser processing of heteroepitaxial GeSn and SiGeSn alloys

Stefan Stefanov, Carlos Conde, Carmen Serra*, Alessandro Benedetti*, Stefano Chiussi
New Materials Group, *CACTI, University of Vigo (Spain)

GeSn and SiGeSn alloys are attractive group IV semiconductor materials with superior carrier mobility, tunable band gaps in the midinfrared with indirect to direct transition above certain composition ranges¹⁻³. The interesting properties of those alloys for independent adjustment of lattice parameters and band gap over a wide range stimulated the research dedicated to CMOS compatible novel device concepts including the combination of Si based with III/V based technologies⁴⁻⁶. Considerable efforts have been recently devoted on growing Ge-rich GeSn and SiGeSn alloys on Si, Ge and InP via MBE and CVD techniques⁷⁻¹⁰. The major problem for incorporating Sn into the Ge is the large lattice mismatch of 4.2% and 19.6% between Si ($a_0=0.5431$ nm) and Ge ($a_0=0.5658$ nm) or α -Sn ($a_0=0.6493$ nm), respectively, the instability of the diamond-cubic structure of α -Sn and the low thermodynamic solubility of Sn in Ge (<1%)¹¹.

Because of these constraints conventional CVD and MBE growth is done at out of equilibrium conditions and low processing temperature that lead to Sn segregation⁷. To counteract these effects and improve the intermixing of the elements in order to obtain binary and ternary Si/Ge/Sn alloys with acceptable crystal quality we propose an alternative, out of equilibrium growth, based on ultra fast (several ns) laser melting/intermixing/epitaxial recrystallization cycles. This technique features low optical absorption depth and well controlled temperature gradient for ultra-rapid heating/cooling cycles, induced by pulses of about 25 ns, which provoke controlled changes in composition and structure of the material. These changes are directly related to the laser processing parameters energy density and number of pulses, thus determine the properties of the final product. An effective control of the experimental parameters is achieved simulating numerically the 1-D spatial thermal depth profile using finite element methods¹²⁻¹⁵. Laser processing of Ge/Sn layers was one of the first routes to metastable GeSn¹⁶ with a strong lack of epitaxy. Pulsed Laser Induced Epitaxy (PLIE) is a technique that improves the epitaxial growth and has already proven to be effective for GeSn and SiGeSn alloys with Sn content below the solubility limits^{14,15,17}.

Virtual Germanium (v-Ge) with different thickness on top of Si has been used for the GeSn and SiGeSn alloys. Sn concentration is controlled varying both processing parameters and the thickness of the top Sn layer deposited on the Ge. This layer was realized either after the v-Ge MBE deposition from Sn effusion cell. GeSn is obtained by intermixing of the Ge and Sn layers, whereas SiGeSn alloying results after intermixing of the Ge and Sn layers with the Si substrate. Samples were irradiated in Ar atmosphere, using 193 nm Excimer Laser (Lambda Physik LPX 220i). The laser beam was spatially homogenized using a fly-eye system (EX-HS-700D) and its energy was "in situ" controlled (Ophir PE50-DIF). Time Resolved Reflectivity (TRR) at 633 nm was used to monitor the phase change duration on the sample surface in real time. Experimental variables were energy density and number of laser shots. Analysis of the samples was performed by Raman spectroscopy (HJY LabRam HR800), TOF-SIMS (IonTOF TOF-SIMS-IV) and RBS.

We started with a comparison of the melt duration extracted from the TRR signal and the one derived from the numerical solution of the heat conduction differential equation. The sample structure used for the numerical simulation was 4 nm Sn on top of 100 nm v-Ge on Si substrate. Melt depth and laser energy density, respectively, were adjusted depending if only the Sn and Ge layers melt (below 104 nm) is wished and GeSn is formed, or if also the Si substrate is included so that the resulting layer forms SiGeSn alloy. The estimated values were 200 mJ/cm² for GeSn and 500 mJ/cm² for SiGeSn (Fig. 1). However, the expected alloys were not obtained with one laser shot of these energy densities. We saw that the level of

intermixing of the corresponding layers (alloy components resp.) was strongly dependent on the number of laser shots (Fig. 2) and therefore samples irradiated with 100 pulses were further studied. Sn substitutional content from RBS yields 1% in GeSn and 0.6% in SiGeSn. We suggest that higher Sn content might be obtained varying Sn and Ge layer thickness that would reflect on the amount of incorporated Sn in both Ge and SiGe.

In summary, we report on an alternative technique to synthesize epitaxial GeSn and SiGeSn alloys and point out a route to reach Sn content above the solubility limit. Also, an improvement of the scalability of the applied technique for GeSn and SiGeSn alloys ranging from micrometer structures to large area substrates is included in this route.

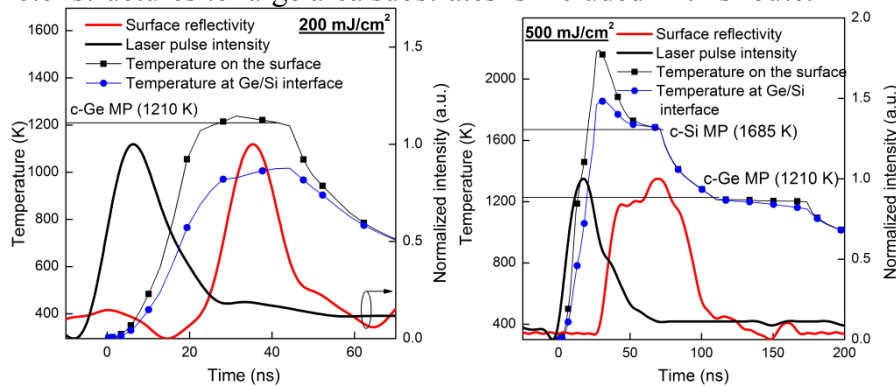


Fig. 1 Comparison of calculated and experimentally obtained melt duration for the first pulse of 200 (left panel) and 500 (right panel) mJ/cm^2 .

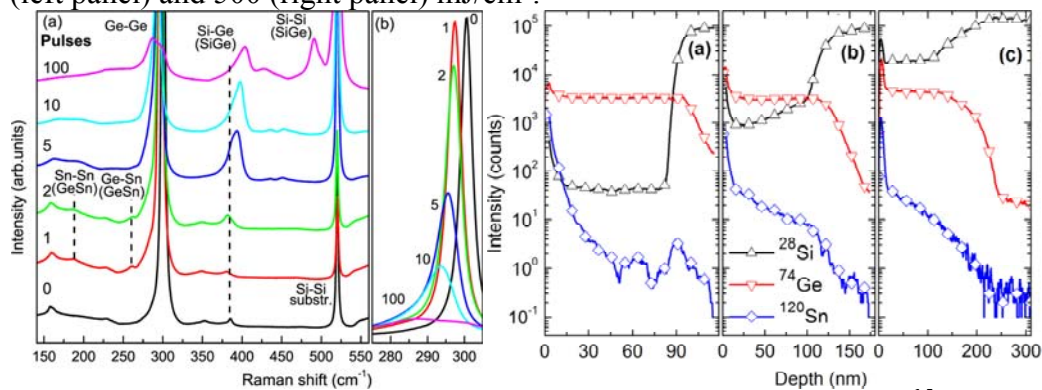


Fig. 2 Evolution of the level of intermixing with increasing number of pulses¹⁵. The left panel (a) shows the transition of the Raman modes from GeSn to SiGeSn for 0 to 100 pulses of $500 \text{ mJ}/\text{cm}^2$, (b) represents the intensity of the Ge-Ge Raman mode that decreases with increasing intermixing of the three components. The right panel shows TOF-SIMS depth profile of the as received (a) irradiated with 5 shots (b) and 100 shots (c) of $500 \text{ mJ}/\text{cm}^2$ samples.

References

- D.W. Jenkins et al., Phys. Rev. B **36**, 7994–8000 (1987).
- K.A. Mader et al., Solid State Communications **69**, 1123 (1989).
- G. Grzybowski et al., App. Physics Letters **99**, 171910 (2011).
- R. Soref et al., Journal of Materials Research **22**, 3281 (2007).
- B. Vincent et al., Microelectronic Engineering **88**, 342 (2011).
- B. Vincent et al., App. Physics Letters **99**, 152103 (2011).
- M. Bauer et al., App. Physics Letters **81**, 2992 (2002).
- J. Werner et al., App. Physics Letters **98**, 061108 (2011).
- Y. Shimura et al., Thin Solid Films **518**, S2 (2010).
- M. Nakamura et al., Thin Solid Films **520**, 3201 (2012).
- J. Kouvetakis et al., Ann. Rev. of Mat. Res. **36**, 497 (2006).
- S. Chiussi et al., Applied Surface Science **254**, 6030 (2008).
- J.C. Conde et al., App. Physics Letters **97**, 014102 (2010).
- S. Stefanov et al., App. Physics Letters **100**, 104101 (2012).
- S. Stefanov et al., App. Physics Letters **100**, 204102 (2012).
- S. Oguz et al., Applied Physics Letters **43**, 848 (1983).
- S. Stefanov et al., Thin Solid Films **520**, 3262 (2012).

Fabrication of Titanium Oxide Nanotube Micro Gas Sensors by Anodization

Yasuo Kimura, Ryota Kojima, Shota Kimura, and Michio Niwano

Laboratory for Nanoelectronics and Spintronics, Research Institute of Electrical
Communication Tohoku University

2-2-1 Katahira, Aoba-ku, Sendai 980-8577, Japan

Tel: +81-22-217-5502 Fax: +81-22-217-5503 E-mail: ykimura@riec.tohoku.ac.jp

The metal oxide semiconductor gas sensor is one of gas sensors and it has useful features of simple structure and high sensitivity. Miniaturization or integration of gas sensors gives a lot of advantages such as low power consumption, improvement of portability, high reliability, and simultaneous measurement of multicomponent. Miniaturization and integration of gas sensors require position controllability and uniformity of materials. It is important to precisely control the position of a device. Therefore, it is important to develop a hybrid process between photolithography and bottom-up process. This requires that the bottom-up process is compatible with photolithography. Then, we used an anodization process, which is compatible with photolithography, as a bottom-up one. The anodization process forms nanotubes with homogenous pore diameter and period. It has been reported that gas sensors using anodic titanium oxide nanotubes have good performance. In this study, we miniaturized metal oxide semiconductor gas sensors using an anodic titanium oxide nanotube film by the hybrid process.

Figure 1 illustrates the miniaturized gas sensor fabrication process. First, a titanium film was deposited on the substrate by DC magnetron sputtering and the titanium film was patterned to form the titanium wire. A protective silicon dioxide layer was deposited on the titanium wire except a region which was anodized. After that the part of the titanium wire was anodized in ammonium fluoride and water containing ethylene glycol solution. Finally, anodic titanium oxide nanotube layer was crystallized. Figure 2 shows the response of the miniaturized hydrogen gas sensor at 300 °C. From Fig. 2, we can see that the conductance change as large as the 20 times when the hydrogen concentration was 10 %. This indicates that a micro gas sensor can be fabricated by the anodization process. Furthermore, the sensed current of about 1 A indicated that a picoamperemeter and formation of interdigitated electrodes are not necessary for sensing current.

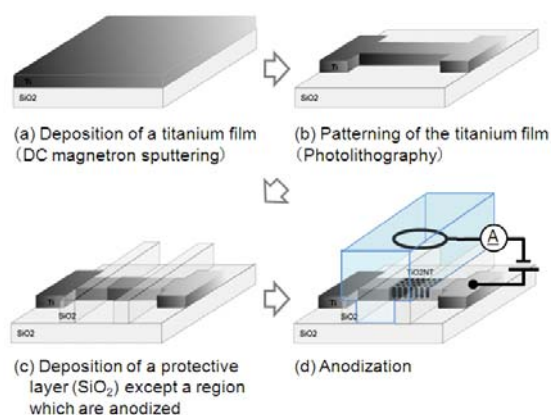


Fig. 1 Fabrication process of micro gas sensors by local anodization of titanium wires

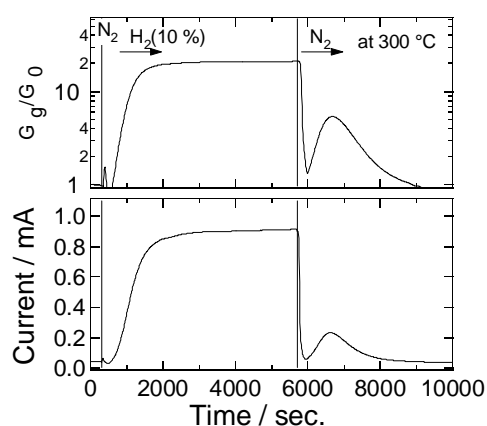


Fig. 2 The response characteristics of a miniaturized hydrogen gas sensor at 300 °C.

Application of titanium oxide nanotube films to solar cells

Michio Niwano, Ryota Kojima, Ma Teng, and Yasuo Kimura

Laboratory for Nanoelectronics and Spintronics, Research Institute of Electrical
Communication Tohoku University

2-2-1 Katahira, Aoba-ku, Sendai 980-8577, Japan

Tel: +81-22-217-5501 Fax: +81-22-217-5503 E-mail: niwano@riec.tohoku.ac.jp

Titanium oxide (TiO_2) nanotubes attracts great interest because of their superior properties such as high photocatalytic activity and high biological affinity, and their application to solar cells, gas sensors and orthopedic implantation have been reported. Anodization of titanium (Ti) is a promising method to fabricate a TiO_2 nanotube film on a substrate because it enables us to form a vertically oriented nanotube structure with uniform diameter and period. On the other hand, dye-sensitized solar cells (DSCs) have been widely studied because of their simple structure and relatively high conversion efficiency. DSCs are composed of a dye-adsorbed TiO_2 nanoparticle film (negative electrode), electrolyte, and a counter electrode and a vertically oriented TiO_2 nanotube film is an alternative to a TiO_2 nanoparticle film because it satisfies the requirements for high energy conversion efficiency: straight current paths and a large surface area to adsorb a lot of dye molecules.

In this study, we fabricated an anodic TiO_2 nanotube film on a transparent conductive oxide (TCO) layer by anodization of a Ti film in an ethylene glycol solution of water and ammonium fluoride (NH_4F). The Ti film was deposited through the DC magnetron sputtering method. The anodization condition was optimized by adjusting electrolyte composition. Figure 1 shows a cross-sectional FE-SEM image of anodic TiO_2 nanotube films formed by anodization of a Ti film at an anodic potential of 40 V in an ethylene glycol solution of 0.2 M NH_4F and 3.0 wt.% water. From Fig.1, we can see that a vertically oriented TiO_2 nanotube film formed on a substrate. The tube diameter was about 90 nm. In addition, a TiO_2 nanotube film was applied to a negative electrode of a DSC as shown in the inset of Fig. 2. The electrolyte of the DSC was a solution of 0.1 M LiI 0.05 M I₂, 0.6 M DMPII, and 0.5 M TBP in acetonitrile. The counter electrode was a platinum thin film sputtered on a TCO layer. Figure 2 shows the I - V characteristic of a DSC using an anodic TiO_2 nanotube film as a negative electrode. This indicates that an anodic TiO_2 nanotube film can be used as a negative electrode of DSC.

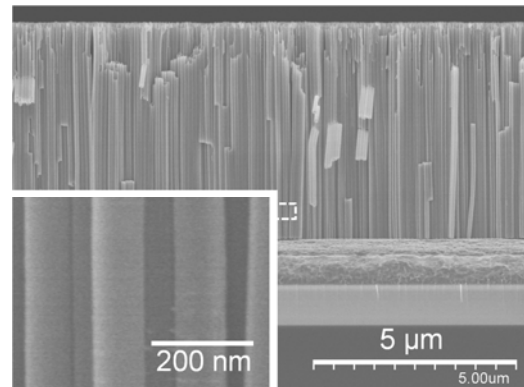


Fig 1 A cross-sectional FE-SEM image of anodic titanium oxide nanotube films formed by anodization of Ti.

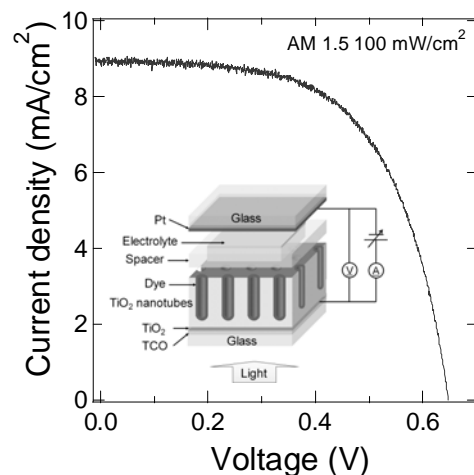


Fig 2 The I - V characteristic of a DSC using an anodic TiO_2 nanotube film as a negative electrode.

Dynamic Characteristics of Neuron Models and Microchip Integration of Active Neural Networks

K. Nakajima

The Laboratory for Brainware/Nanoelectronics and Spintronics,
Research Institute of Electrical Communication, Tohoku University
2-1-1 Katahira Aobaku Sendai Japan, +22-217-5558, hello@riec.tohoku.ac.jp

There have been many researches of various neuron models which typically take the form of ordinary nonlinear differential equations of several dimensions. The pattern of spiking is of great importance, because it is believed that it codifies the information transmitted by neurons. It is an actively studied problem to apply various neuron models to artificial neural networks (ANNs) for intelligent information processing in the field of nonlinear dynamics and the brain research.

One of important aspects of this situation is the lack of universal discussion over the dynamical behaviors of various neuron models, though perturbation and bifurcation theories exist. Thus we reveal that each model has its own potential function and active areas on the potential. Negative resistance is one of active areas. This concept realizes the universal discussion of the dynamical behaviors of models, for example, bursting, spiking, etc.

On the other hand, Hopfield neural network is capable of solving combinatorial optimization problems and it is a parallel-processing version of the gradient method. However, it has some drawbacks. One of the most concerning drawbacks is that it frequently finds locally minimum solutions instead of global minima.

The active areas of neuron models make the state of network escape from local minima by their destabilization. In computer simulation and theoretical estimation, we have already shown that the ID network, which is one of active ANNs to implement associative memory and combinatorial optimization problems, is capable of converging on optimal solutions only.

The prototype chip of a burst ID model, which shows bursting dynamics as an extended version of the ID model, has been fabricated and measured.

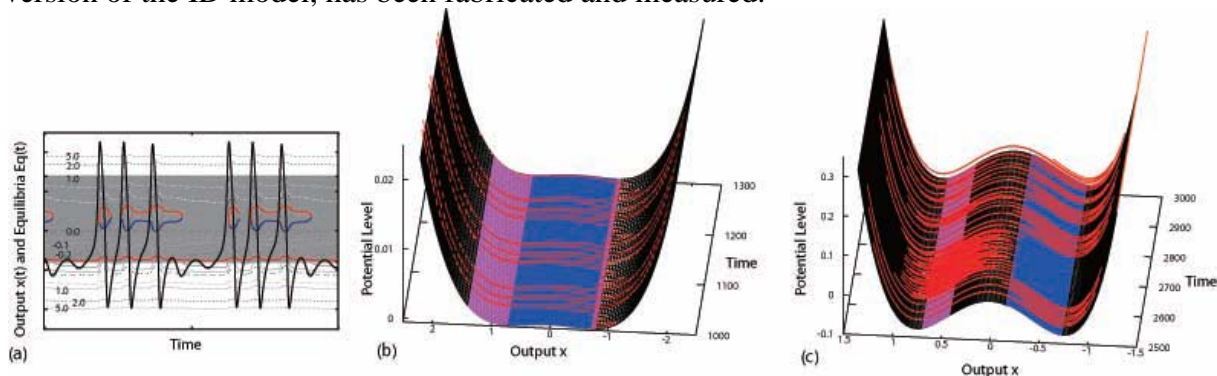


Fig. 1 Burst and chaotic oscillations bound by the potential with the active areas. (a) Time series of output on a contour map of the potential. Bird's eye views of outputs on the potentials, (b) for a burst oscillation and (c) for a chaotic oscillation.

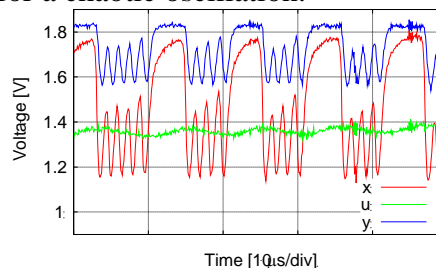
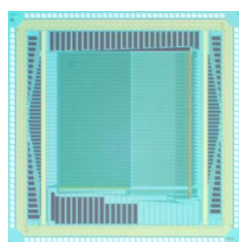


Fig. 2 Photograph of a microchip for the Burst-ID ANN, and an observed bursting output.

Ionic Liquid-Gated Organic Field-Effect Transistors

Shohei Iino, Yasuo Kimura, and Michio Niwano

Laboratory for Nanoelectronics and Spintronics, Research Institute of Electrical
Communication Tohoku University

2-2-1 Katahira, Aoba-ku, Sendai 980-8577, Japan

Tel: +81-22-217-5502 Fax: +81-22-217-5503 E-mail: iino@riec.tohoku.ac.jp

An ionic liquid-gated organic transistor can drive high output current at a low voltage compared with a general organic field effect transistor (OFET). It is necessary to elucidate the operation mechanism for improvement of the performance of ionic liquid-gated organic transistors. Two operation mechanisms of ionic liquid-gated organic transistors have been proposed. One is carrier generation due to electrochemical doping. The other is accumulation of a great number of carriers due to formation of an electric double layer, which functions as a very thin gate insulator. However, it is difficult to distinguish these mechanisms. In this study, the generation of carriers in a P3HT layer was in-situ observed using infrared absorption spectroscopy in the multiple internal reflection geometry (MIR-IRAS).

Figure 1 illustrates the structure of an ionic liquid-gated organic transistor. A gate insulator layer was replaced with ionic liquid. P3HT and [BMIM][PF₆] were used as an organic layer and ionic liquid, respectively. The thickness of a P3HT layer was 15 nm. Figure 2 shows the typical output characteristic of ionic liquid-gated organic transistors. The gate length and width were 2 μm and 1 mm, respectively. From Fig. 2, it can be seen that a large drain current of 0.7 mA flew when a gate voltage was 1.5 V and an ionic liquid-gated organic transistor can drive large current. Figure 3 shows infrared spectra or (a) a P3HT layer of the ionic liquid-gated organic transistor during operation and (b) a FeCl₃-doped P3HT film [1]. The P3HT layer was 3 μm in thickness. It was thick enough to observe penetration of PF₆⁻ to the P3HT layer because it was much thicker than the penetration depth of the evanescent field of infrared. From Fig. 3, we can see that intensities of infrared absorption peaks due to P3HT cation increased with an increase in the gate voltage. This indicates that PF₆⁻ penetrated into the P3HT layer to generate carriers, that is, electrochemical doping took place.

[1] Y. Furukawa, *Synth. Met.* **135-136** (2003) 341.

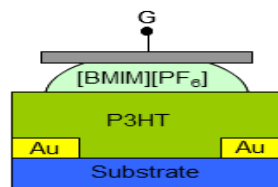


Fig 1 The structure of an ionic liquid-gated organic transistor.

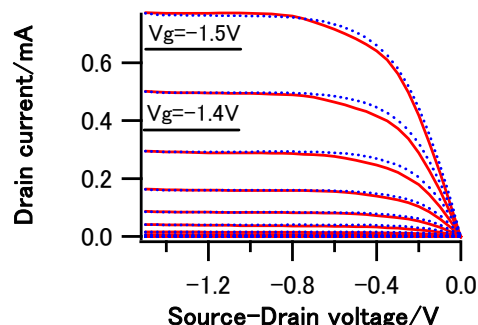


Fig 2 A typical output characteristic of ionic liquid-gated transistor.

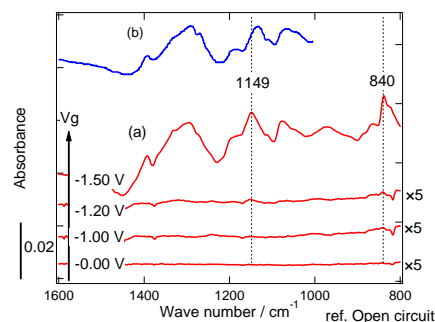


Fig 3 Infrared spectra for (a) a P3HT layer of the ionic liquid-gated organic transistor during operation and (b) a FeCl₃-doped P3HT film [1].

UV Excimer laser processing of SiGe and SiGeSn: finite elements method numerical modeling

Stefan Stefanov, Carlos Conde, Elena Martín, Julia Serra, Pio González, Stefano Chiusi
New Materials Group, University of Vigo (Spain)

During the years, Pulsed Laser Induced Epitaxy (PLIE) has always been the “alternative” for epitaxial formation of group IV alloys with great variety of intermixed components, ranging from SiGe¹⁻³, SiC⁴, SiGeC⁵⁻⁷ to GeSn⁸⁻¹⁰ and SiGeSn^{9,11,12}. First Abelson et al.¹ was able to overcome the drawback of PLIE, called “cellular” structure growth^{8,13} for SiGe and our group for GeSn⁹ (for the given bellow configuration), resulting epitaxial abrupt or tailored concentration Si/Ge/Sn layers. The process itself consists of ultra rapid (up to several hundred ns) pulsed laser heating/cooling of the alloy components previously deposited in form of a multilayer structure and a crystalline substrate followed by epitaxial growth and solidification of the mixture.

Numerical simulation of the laser/material interaction has been widely used, mainly in high power lasers processing, to predict and fine tune the optimal experimental conditions^{14,15}. Same approach was later transferred to PLIE processing of group IV elements¹⁶ and alloys^{10,12,17,18}. In general, it consists of Finite Elements Method (FEM) solution of the Heat Conduction Differential Equation (HCDE) for given boundary conditions and known heat gradient devoted from the Beer–Lambert law. The FEM analysis yields the values of the maximum melting depth (MMD) and melts duration (MD) for each mesh element. Those parameters can be extracted directly compared with experimental ones after sample characterization. MD or liquid phase monitoring, the so called Time Resolved Reflectivity (TRR), of the ultra rapid PLIE process yields essential experimental information correlated to the level of intermixing and thus composition^{1,9,19}. It can be easily obtained with the simple experimental setup shown on figure 1 (left). Fig. 1 (right) represents good agreement of the TRR signal with the data obtained from the FEM analysis of 4 nm Sn/100 nm Ge/Si(100) multilayer. This paper aims to represent our approach to FEM analysis of group IV elements PLIE processing in general and our latest results concerning GeSn and SiGeSn alloys.

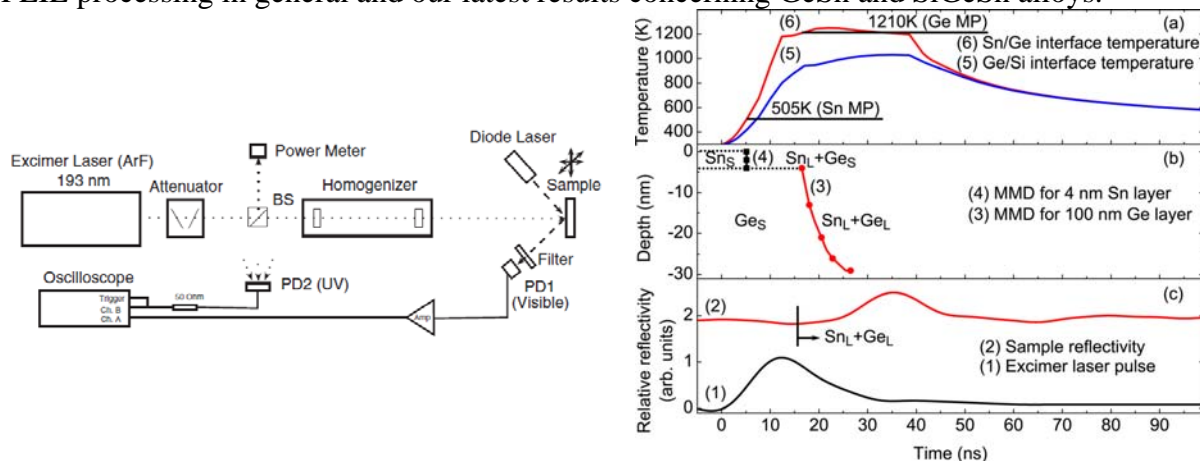


Fig. 1 Experimental PLIE/TRR setup (left). Temporal evolution of the (a) interface temperatures, (b) depth of solid-liquid transition, and (c) reflectivity, caused by the first laser pulse of 200 mJ/cm² (right).

¹ J.R. Abelson et al., Applied Physics Letters **52**, 230 (1988).

² S. Martelli et al., Journal of Applied Physics **82**, 147 (1997).

³ N. Frangiset al., Applied Physics Letters **72**, 2877 (1998).

⁴ K.M. Kramer et al., Journal of Applied Physics **79**, 4118 (1996).

⁵ K.-J. Kramer et al., Applied Surface Science **69**, 121 (1993).

⁶ J. Boulmer et al., Journal of Crystal Growth **157**, 436 (1995).

⁷ E. López et al., Thin Solid Films **508**, 48 (2006).

⁸ S. Oguz et al., Applied Physics Letters **43**, 848 (1983).

⁹ S. Stefanov et al., Thin Solid Films **520**, 3262 (2012).

¹⁰ S. Stefanov et al., Applied Physics Letters **100**, 104101 (2012).

¹¹ G.H. Wang et al., Applied Physics Letters **91**, 202105 (2007).

¹² S. Stefanov et al., Applied Physics Letters **100**, 204102 (2012).

¹³ I. Golecki et al., Thin Solid Films **57**, L13 (1979).

¹⁴ H.E. Cline et al., Journal of Applied Physics **48**, 3895 (1977).

¹⁵ J. Ascough, Optics and Lasers in Engineering **6**, 137 (1985).

¹⁶ S. de Unamuno et al., Applied Surface Science **36**, 1 (1989).

¹⁷ J.C. Conde et al., Applied Surface Science **248**, 461 (2005).

¹⁸ L. Fornarini et al., Applied Surface Science **254**, 898 (2007).

¹⁹ J. Solis et al., Journal of Applied Physics **69**, 2105 (1991).

Ion doped apatite coatings by laser ablation

C. Rodríguez-Valencia, M. López-Alvarez, E.L. Solla, D. Cordero, H. Aguiar, J. Serra,
S. Chiussi, P. González
Applied Physics Dpt., University of Vigo, Spain
Campus Lagoas-Marcosende, 36208 Vigo, Spain, telephone: 0034986812216,
fax: 0034986812201, e-mail: pglez@uvigo.es

The mineral family of apatites presents the property of being able to incorporate a variety of ions and compounds into its structure [2]. Hydroxyapatite, $\text{Ca}_{10}(\text{PO}_4)_6(\text{OH})_2$ (HA), is a member of the apatites group which has been investigated extensively as a biomaterial due to its resemblance to the inorganic phase of bone. The growing evidence of the beneficial role of different ions (Si , Se , Mg^{2+} , K^+ , Na^+ , F^- , Sr^{2+} , ...) in bone tissue has increased the interest of developing ion doped apatites for medical applications, and specifically biocompatible coatings that can be deposited on metallic implants to benefit from their loadbearing capabilities, protection against the release of metal ions into the body and improvement of the implant fixation to hard tissues.

Pulsed laser deposition (PLD) is a technique that has proven effective in the fabrication of calcium phosphate films on metallic substrates with excellent final coating attachment. It makes use of laser pulses to expel target material from a rotating disk placed inside a vacuum reaction chamber and project it on the surface of a metallic substrate. The PLD method outperforms other techniques in versatility, since the choice of its ablation and deposition parameters control of the stoichiometry and crystallinity of the deposited material.

Ion doped hydroxyapatite (*i*HA:Si,Sr,Se) coatings have been fabricated by pulsed laser deposition (PLD) from initial targets obtained after mixing and compacting commercial HA and different proportions of precursors powders. The macroscopic morphology of the films presented in all cases equivalent spherical shaped aggregates of typical calcium phosphate coatings (see an example in Fig. 1). The incorporation of different ions (silicon, selenium, and strontium) into the HA compounds follows a linear behavior with the composition of the precursor compound in the original ablation target (Figs. 2 and 3).

Additionally, the coatings thus fabricated were structurally, morphologically and chemically characterized using scanning electron microscopy, optical profilometry, X-ray diffraction, Fourier-transform infrared spectroscopy, X-ray photoelectron spectroscopy and energy dispersive X-ray spectroscopy. The role of the ion doped in the modification of the HA structure and possible substitutional mechanisms are discussed.

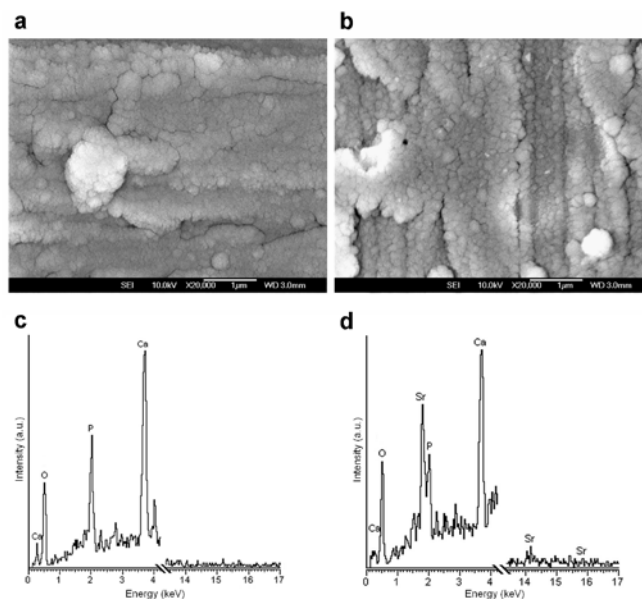


Fig. 1 SEM micrographs and EDS analysis of two representative coatings deposited on titanium: pure HA (a,c) and *iHA:Sr* produced from an ablation target of 10% Sr (b,d).

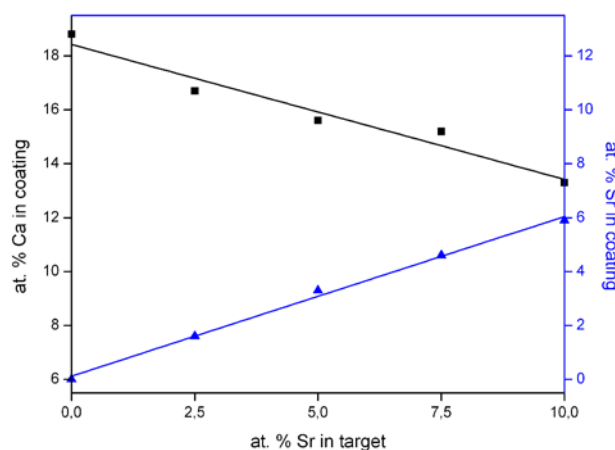


Fig. 2 Incorporation of Sr (▲) in the coating measured by XPS as a function of the at. % of Sr in the target, and consequent decremental effect of the Ca (■) content in the coatings.

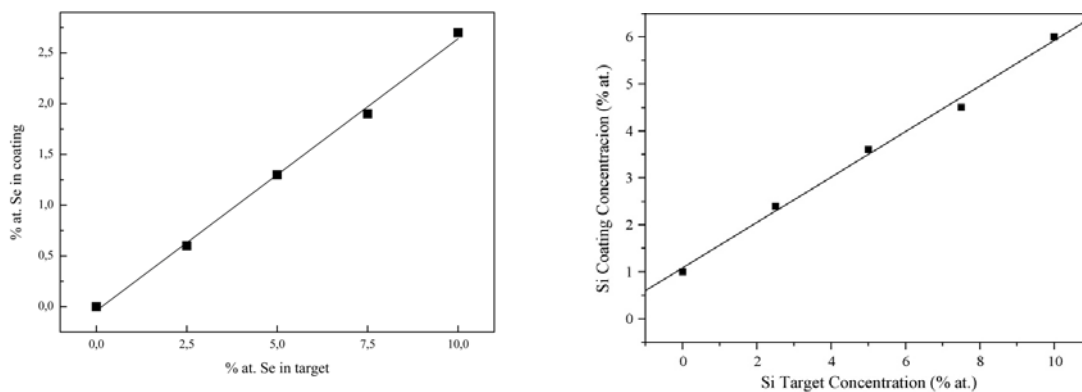


Fig. 3 Similar behaviors were found for *iHA:Si* and *iHA:Se* coatings obtained by laser ablation.

Innovative porous SiC ceramics from natural precursors

M. López-Álvarez, C. Rodríguez-Valencia, S. Chiussi, J. Serra, P. González.

Applied Physics Dpt, Campus Lagoas-Marcosende 36310, University of Vigo,
Spain. Telephone number +34 986812216. Fax number: +34 986812201. Email address:
miriammsd@uvigo.es

Silicon carbide (SiC) belongs to the materials known as advanced ceramics which emerged as a consequence of the limitations of metal alloys for certain structural applications or in aggressive environments at high temperatures^{1,2}. It is a low dense material (3.21g/cm^3) composed by a covalent bond, covalence degree of 88%, and a similar structure to diamond. Both properties are the reasons for presenting a value of hardness of 13 in Mohr scale (being 15 for diamond¹) as well as a great mechanical strength to both thermal shock and chemical attack³. At the same time, due to its electron configuration it acts as a semiconductor material. Silicon carbide can be obtained by different traditional methods as hot pressing sintering, pressureless sintering, chemical vapor deposition etc. The main drawbacks of the prior techniques are the complexity in the reproducibility of the pieces and the difficulty to obtain complex shapes, which reduces the range of applicability of the ceramics, the need for final machining and high temperatures requiring of expensive technology (high cost of manufacture) and the decrease of mechanical properties due to the use of additives^{1,3}.

In 2001 a new method for the obtaining of SiC was developed⁴. This process met the requirements for all industrial manufacturing processes that are low cost and simplicity and, included the novel use of biological plant precursors as the carbon source⁴. It consists on the pyrolysis, or thermal decomposition, of the cellulose-based precursor to obtain a piece of porous carbon that preserves on it the interconnected vascular system of the plant. This piece of carbon is then subjected to a reactive infiltration with silicon (up to 1550°C). The molten silicon will flow through the entire piece by means of the interconnected pores reacting with carbon, resulting in a porous SiC ceramic, also called Biomorphic[®] SiC¹. The use of silicon powder of high purity or additives are not necessary and, due to the use of an open-porosity structure, the velocity of the synthesis increases together with the ability to produce pieces with complex shapes by modeling the carbon preform¹.

Different cellulose-based precursors as trees (*Entrandrophragma cylindricum*, *Eucalyptus* spp and *Pinus* spp), marine plants (*Juncus maritimus* and *Zostera marina*) or macroalgae species (*Laminaria ochroleuca*) have been successfully used for the obtaining of these porous SiC ceramics. The fact that the final ceramic retains the biological porosity and interconnectivity is one of the reasons for the great potential of this material, as traditionally it has been “printed” on the different materials the specific needed microstructure. With the use of these plant precursors, that costly process is avoided given that the desired microstructure has been already developed on the materials by nature⁶, providing the ceramics with macro- and micro-patterning on their surfaces, ranges of porosity from nano to macro-scale... that will make it possible to select one over another depending on the final application⁵. Thus, it has been introduced in industrial processes as a compound resistant to abrasion and corrosion (mechanical valves), to friction (brake pads), to temperature (receivers of solar radiation, engines, turbines), also in structural reinforcing concretes, acoustic and thermal isolation... or even as a biomaterial for bone prosthesis^{1,5,7}. As a semiconductor material it is also attractive for blue light emitting diodes, ultraviolet and high-temperature sensors, radiation-hardened electronics, high-power electronics... This work pretends to summarize the great variety of materials with a range of microstructures and porosities that these biological precursors have provided to the ceramics field.

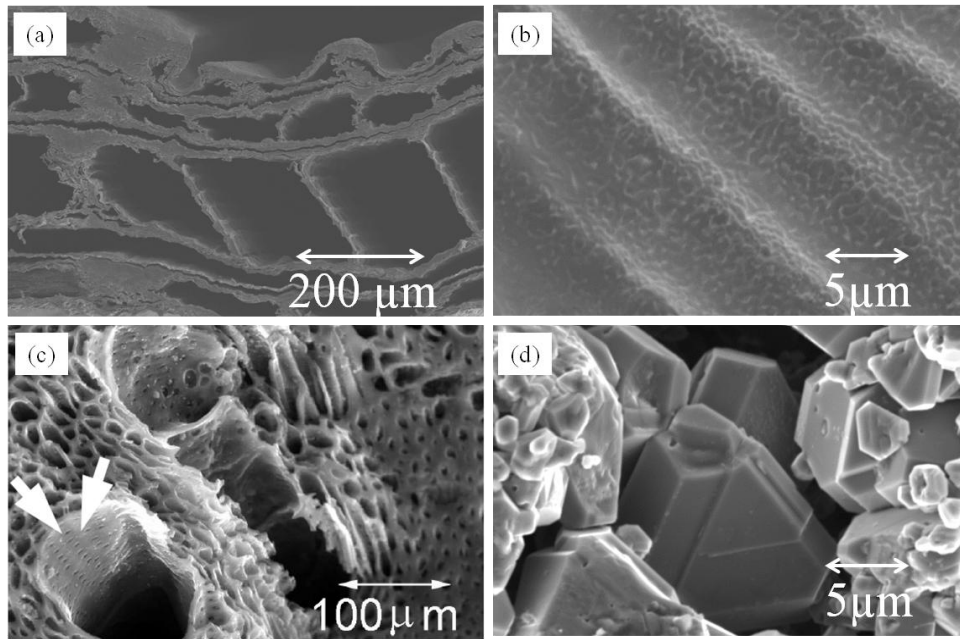


Fig. 1 Scanning electron micrographs presenting porosity (a, c), surface patterning (b) of different cellulose-based precursors and a crystal of silicon carbide (d).

References

1. Varela-Feria *et al.* 2002. *Ceram Eng Sci Proc* 23: 681-687.
2. Teixeira. 2005. PhD Dissertation. Faculdade de Engenharia. Universidade do Porto.
3. González *et al.* 2003. *Biomaterials* 24:4827:4832.
4. Martínez-Fernández *et al.* 2001. Patent P200102278.
5. Martínez Fernández *et al.* 2000. *Scripta Mater* 43:813-818.
6. Varela Feria *et al.* 2002. *Bol Soc Esp Cerám Vid.* 41: 377-384.
7. De Arellano López *et al.* 2004. *Int J Appl Ceram Tech* 1:1-12.